

Theory of magnetic flux tubes in strong fields and the phenomenon of dark matter axions identical to solar axions

Vitaliy D. Rusov* and Vladimir P. Smolyar

*Department of Theoretical and Experimental Nuclear Physics,
Odessa National Polytechnic University, Odessa, Ukraine*

Margarita E. Beglaryan

*Department of Computer Technology and Applied Mathematics,
Kuban State University, Krasnodar, Russia*

(Dated: September 7, 2021)

We develop the general laws of the theory of the almost empty anchored magnetic flux tubes (MFT) with $B \sim 10^7 G$, starting from tachocline to the surface of the Sun. The main result of this theory is the formation of the solar axions and the magnetic O-loop inside the MFT near the tachocline. In this magnetic O-loop (based on the Kolmogorov turbulent cascade) the axions are converted to photons, producing the axion origin photons near the bottom of the convective zone, i.e. near the tachocline. On the other hand, high-energy photons from the radiation zone through the axion-photon oscillations in the O-loop inside the MFT near the tachocline produce the so-called axions of photon origin under the sunspot. This means that at such strong magnetic fields the Parker-Biermann cooling effect of MFT develops due to the “disappearance” of the Parker’s convective heat transport, and consequently, the temperature in the lower part of the magnetic tube with the help of the axions of photonic origin from the photon-axion oscillations in the O-loop near the tachocline. As a result, a free path for photons of axion origin opens from the tachocline to the photosphere!

We show that the width of the ring between the magnetic wall of the flux tube and the magnetic O-loop near the tachocline, is the distance between the Parker-Biermann cooling effect, which forms the flux tube buoyancy, and the convective heating source $(dQ/dt)_2$, which, despite the neutral buoyancy of the magnetic tube ring, repeats the upstream tube identically. In other words, the source of convective heating $(dQ/dt)_2$ appears on the surface of the Sun as a result of the initiation (due to the Parker-Biermann cooling effect) of adiabatic growth of an undulatory instability in toroidal flux tubes which initially were in mechanical equilibrium (neutral buoyancy) in the stable overshoot layer.

A very beautiful problem was solved this way. The high-energy photons passing from the radiation zone through the horizontal field of the O-loop near the tachocline turn into axions (see inverse oscillations $\gamma + \vec{B} \rightarrow \vec{B} + a$), which almost completely eliminates the radiation heating $(dQ/dt)_1$ of the almost empty magnetic flux tube. A certain flux of photons coming from the radiation zone through the tachocline, passes through the “ring” of a strong magnetic tube by virtue of convective heating $(dQ/dt)_2$. It allows to determine both the velocity and the lifetime of the magnetic flux tube (with $B \sim 10^7 G$) before the reconnection, from tachocline to the surface of the Sun, as well as the rate of the magnetic flux tube reconnection (with $B \sim 10^5 G$) near the tachocline V_{rec} . The latter is determined only by the rise time of the magnetic loop and the disappearance of the spot from the surface of the Sun.

Finally, we can show that the formation of sunspot cycles is equivalent to the number of cycles from the MFT, which coincides with the observational data of the Joy’s law, and that both effects are the manifestations of dark matter (DM) – solar axions in the core of the Sun, whose modulations are controlled by the anticorrelated 11-year modulation of asymmetric dark matter (ADM) density in the solar interior.

I. INTRODUCTION AND MOTIVATION

It is known that the unsolved problem of energy transport by magnetic flux tubes at the same time represents another unsolved problem related to the sunspot darkness (see 2.2 in [1]). Of all the known concepts playing a noticeable role in understanding the connection between the energy transport and sunspot darkness, let us consider the most significant theory, in our view. It is based

on the Parker-Biermann cooling effect [2–4] and originates from the early works of Biermann [3] and Alfvén [5].

As you know, the Parker-Biermann cooling effect [2–4], which plays a role in our current understanding, originates from Biermann [3] and Alfvén [5]: in a highly ionized plasma, the electrical conductivity can be so large that the magnetic fields are frozen into the plasma. Biermann realized that the magnetic field in the spots themselves can be the cause of their coolness – it is colder because the magnetic field suppresses the convective heat transport. Hence, the darkness of the spot is due to a

* Corresponding author e-mail: siis@te.net.ua

decrease in surface brightness.

Parker [2, 4, 6–8] has pointed out that the magnetic field can be compressed to the enormous intensity only by reducing the gas pressure within the flux tube relative to the pressure outside, so that the external pressure compresses the field. The only known mechanism for reducing the internal pressure sufficiently is a reduction of the internal temperature over several scale heights so that the gravitational field of the Sun pulls the gas down out of the tube (as described by the known barometric law $dp/dz = -\rho g$). Hence it appears that the intense magnetic field of the sunspot is a direct consequence of the observed reduced temperature [2].

On the other hand, Parker [8, 9] has also pointed out that the magnetic inhibition of convective heat transport beneath the sunspot, with the associated heat accumulation below, raises the temperature in the lower part of the field. The barometric equilibrium leads to enhanced gas pressure upward along the magnetic field, causing the field to disperse rather than intensify. Consequently, Parker [8] argued that the temperature of the gas must be influenced by something more than the inhibition of heat transport!

Our unique alternative idea is that the explanation of sunspots is based not only on the suppression of convective heat transfer by a strong magnetic field [3] through the enhanced cooling of the Parker-Biermann effect [6], but also on the appearance of the axions of photonic origin (Fig 5, Fig. B.1 in [10]) from the tachocline to the photosphere, which is confirmed by the “disappearance” of the heat, and consequently, the temperature in the lower part of the magnetic tube [8, 9] due to the axions of photonic origin from the photon-axion oscillations in the O-loop near the tachocline (see Fig. 5).

This means that the appearance of axions of photonic origin, which “remove” the problem of the temperature rise in the lower part of the magnetic tube, and the photons of axionic origin, which have the free path (Rosseland length; see Fig. B.3 in [10]) from the tachocline to the photosphere, are the explanation of sunspots based not only on the suppression of convective heat transport by a strong magnetic field [3], but also on the indispensable existence of the Parker-Biermann cooling effect.

On the other hand, we understand that the existence of the Parker-Biermann cooling effect is associated with the so-called thermomagnetic Ettingshausen-Nernst effect (see Appendix A in [10]).

Due to the large temperature gradient in the tachocline, the thermomagnetic EN effect [11–14] creates electric currents that are inversely proportional to the strong magnetic field of the tachocline. As we showed earlier [10], the toroidal magnetic field of tachocline by means of the thermomagnetic Ettingshausen-Nernst effect (Appendix A) “neutralizes” the magnetic field of the solar core $\sim 5 \cdot 10^7 G$ [15, 16]. It means that, using the thermomagnetic EN effect, a simple estimate of the magnetic pressure of an ideal gas in the tachocline of e.g. the Sun,

$$\frac{B_{tachoc}^2}{8\pi} = p_{ext} \approx 6.5 \cdot 10^{13} \frac{erg}{cm^3} \text{ at } 0.7R_{Sun}, \quad (1)$$

can indirectly prove that by using the holographic principle of quantum gravity (see Appendix C in [10]), the repelling toroidal magnetic field of the tachocline exactly “neutralizes” the magnetic field in the Sun’s core (see Fig. A1 in [10])

$$B_{tachoc}^{Sun} = 4.1 \cdot 10^7 G = -B_{core}^{Sun}, \quad (2)$$

where the projections of the magnetic fields of the tachocline and the core have equal values but opposite directions.

Such strong magnetic fields in a tachocline of e.g. the Earth, Sun, magnetic white dwarfs, accreting neutron stars and BHs can predict the exact “neutralization” of the magnetic field in the core of these stars and in a black hole (see Appendix C in [10]).

Let us note another important Babcock-Leighton (BL) mechanism. On the one hand, we mark out the holographic BL mechanism (see Fig. C.1b in [10]), which we often refer to as the holographic antidynamo mechanism, caused by a remarkable example of the Cowling antidynamo theorem. This theorem states that no axisymmetric magnetic field can be maintained through the self-sustaining action of the dynamo by means of an axially symmetric current [17]. On the other hand, the holographic BL mechanism (as a component of our solar antidynamo model) follows our example of a thermomagnetic EN effect, or the so-called solar holographic antidynamo, in which the poloidal field originates directly from the toroidal field, but not vice versa (see Fig. C.1a in [10]).

Using the Babcock-Leighton mechanism (see Fig. 1), and consequently, the MFT in strong fields, we are interested in the existence of dark matter axions identical to solar axions, which strongly affects the magnetic O-loops inside the MFT near the tachocline, and is thus connected to the so-called thermomagnetic Ettingshausen-Nernst effect through the Parker-Biermann cooling effect (see Appendix A in [10]).

Since the photons of axion origin cause the Sun luminosity variations, then unlike in the case of the self-excited dynamo, an unexpected yet simple question arises: is there a dark matter chronometer hidden deep in the Sun core?

In order to answer this question, let us first consider all the unexpected and intriguing implications of the 11-year modulations of the ADM density in the solar interior and around the BH (see Sect. 3 in [10]).

A unique result of our model is the fact (see Sect. 3 in [10]), that the periods, velocities and modulations of the S-stars are the essential indicator of the modulation of the ADM halo density in the fundamental plane of the Galaxy center, which closely correlates with the density modulation of the baryon matter near the SMBH. If the

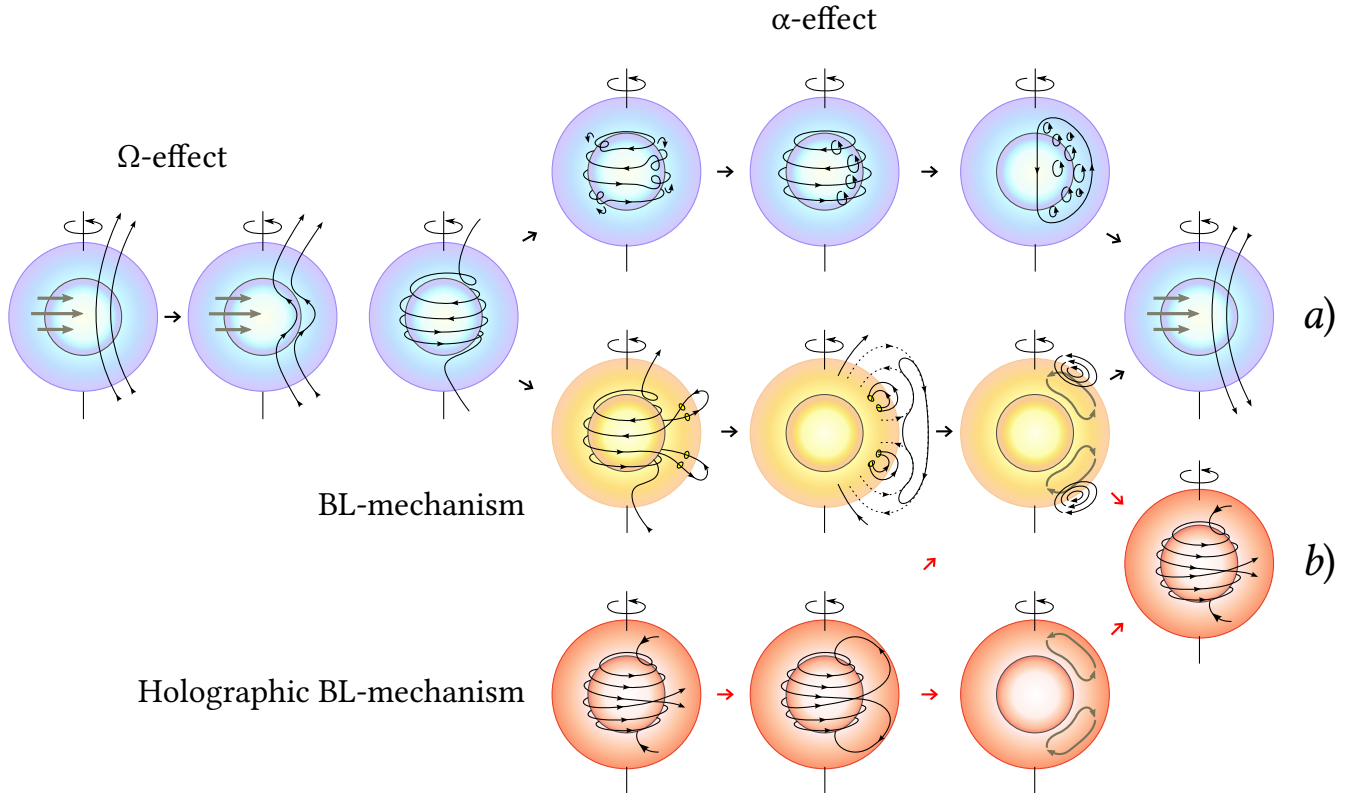


FIG. 1. An illustration of the main possible processes of a magnetically active star of the Sun type. (a) α -effect, Ω -effect and BL mechanism as components of the solar dynamo model. The Ω -effect (blue) depicts the transformation of the primary poloidal field into a toroidal field by differential rotation. Regeneration of the poloidal field is then performed either by the α -effect (top) or by the BL mechanism (yellow in the middle). In case of α -effect, the toroidal field at the base of the convection zone is subject to cyclonic turbulence. In the BL mechanism, the main process of regeneration of the poloidal field (based on the Ω -effect (blue)) is the formation of sunspots on the surface of the Sun from the rise of floating toroidal flux tubes from the base of the convection zone. The magnetic fields of these sunspots closest to the equator in each hemisphere diffuse and join, and the field due to the spots closer to the poles has a polarity opposite to the current that initiates rotation of the polarity. The newly formed polar magnetic flux is transported by the meridional flow to deeper layers of the convection zone, thereby creating a new large-scale poloidal field. Derived from [18]. (b) BL mechanism and holographic BL mechanism as components of our solar antidynamo model. Unlike the component of the solar dynamo model (a), the BL mechanism, which is predetermined by the fundamental holographic principle of quantum gravity, and consequently, the formation of the thermomagnetic EN effect (see [19–21]), emphasizes that this process is associated with the continuous transformation of toroidal magnetic energy into poloidal magnetic energy ($T \rightarrow P$ transformation), but not vice versa ($P \rightarrow T$). This means that the holographic BL mechanism is the main process of regeneration of the primary toroidal field in the tachocline, and thus, the formation of floating toroidal magnetic flux tubes at the base of the convective zone, which then rise to the surface of the Sun. The joint connection between the poloidal and toroidal magnetic fields is the result of the formation of the so-called meridional magnetic field, which goes to the pole in the near-surface layer, and to the equator at the base of the convection zone. Adopted from [10]

modulations of the ADM halo at the GC lead to modulations of the ADM density on the surface of the Sun (through vertical density waves from the disk to the solar neighborhood), then there is an "experimental" anticorrelation identity between such indicators as the ADM density modulation in the solar interior and the number of sunspots. Or equivalently, between the modulation of solar axions (or photons of axion origin) and the sunspot cycles!

A hypothetical pseudoscalar particle called axion is

predicted by the theory related to solving the CP-invariance violation problem in QCD. The most important parameter determining the axion properties is the energy scale f_a of the so-called U(1) Peccei-Quinn symmetry violation. It determines both the axion mass and the strength of its coupling to fermions and gauge bosons including photons. However, in spite of the numerous direct experiments, axions have not been discovered so far. Meanwhile, these experiments together with the astrophysical and cosmological limitations leave a rather

narrow band for the permissible parameters of invisible axion (e.g. $10^{-6}eV \leq m_a \leq 10^{-2}eV$ [22, 23]). The PQ mechanism, solving the strong CP problem in a very elegant way [24, 25], is especially attractive here, since the axion is also a candidate for dark matter [26–29].

Let us first make some clarifications. Various cosmological theories of dark matter (cold, warm, hot) do not relate to the temperature of the matter itself, but to the abundance and concentration of dark matter haloes on a subgalactic scale, on which the fundamental physics of dark matter depends on the so-called free streaming length (FSL) of dark matter [30–32]). Hence, we understand that the smaller the mass of dark matter particles, the warmer they are and the faster they move. It means that the hot dark matter is composed of very light particles with high FSL, e.g. the axions emitted in the inflation of the Universe [33] or from the cores of supernovae [34] and even the Sun [10]. From here, we understand that, according to Co & Harigaya [33], the axions of hot dark matter are the inflationary source of the baryons and leptons formation, while in post-inflation, “the collisions and interactions between gas-rich galaxies are thought to be pivotal stages in their formation and evolution, causing the rapid production of new stars” [35], emitting streams the axions of hot dark matter (e.g. supernovae [34], Galactic Globular Clusters [36] and the Sun [10]). On the other hand, the post-inflationary cold dark matter, composed of massive particles, will be the main source of cold dark matter halos with low FSL, for example, the ADM halo (see e.g. [10, 37]).

From here, we know that if a dark matter particle is considered as a field quantum which participates only in gravitational interaction, then we should call the axions with the same values of the axion-photon coupling $g_{a\gamma}$ and the mass m_a (see the red star in Fig. 2) the dark matter axions, which can move with some “free streaming length” (FSL). It means that the same axions can be the hot dark matter with high FSL, for example, on the Sun (see e.g. [37]), or the axions of cold dark matter with low FSL in our galactic halo, although the density of the axion component is insignificant in the ADM halo (see [10]).

For a fundamental test of a dark matter particle that participates only in gravitational interaction, we will use the test in such a way as to make the axion, surprisingly, visible, using the idea of the remarkable physicist Sikivie [29, 42], which exploits the coupling of the axion to the electromagnetic field through the gravitational interaction of axions with the addition of the so-called great unification of the strong and electroweak interactions. This way the problem of the dark matter axion may be solved on the basis of the physics of axions on the Sun with the help of the helioscopes, and axions in our galaxy with the help of the haloscope.

For now, the problem of dark matter axions is solved using e.g. helioscopes [39]) and haloscopes [40, 41] (see red star in Fig. 2), which may finally solve this problem,

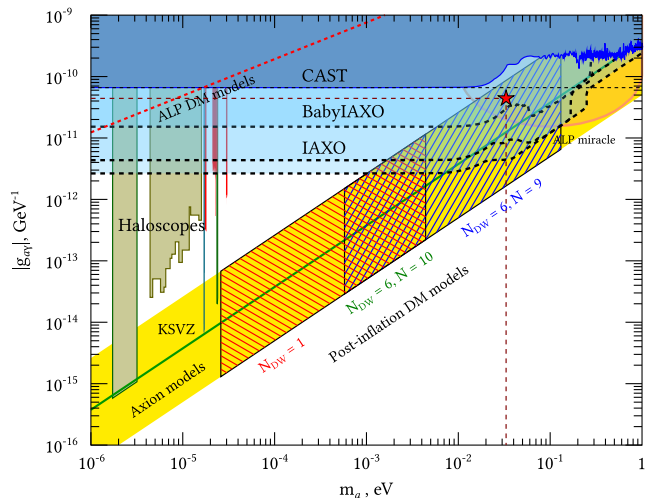


FIG. 2. Predicted mass ranges in which QCD axions can account for the observed cold DM abundance in the post-inflationary PQ symmetry breaking scenario. The generic prediction of QCD axion models is shown in the yellow region. The sensitivity prospects of IAXO are also plotted. The prediction of the post-inflationary PQ symmetry breaking scenario differs according to the value of N_{DW} and the structure of the explicit symmetry breaking terms in the models with $N_{DW} > 1$: N_{DW} is the colour-anomaly of the PQ symmetry, which turns out to be a positive integer and it is called the “domain wall number” in this context. Dashed regions correspond to the predictions (up to uncertainties in the estimation of the relic axion abundance) of the models with $N_{DW} = 1$ (red), $N_{DW} = 6$ and $N = 9$ (blue), and $N_{DW} = 6$ and $N = 10$ (green). Adopted from [38]. The vertical green lines are from [39] and [40], three red lines are from [41]. The red star marks the axion mass $m_a \sim 3.2 \cdot 10^{-2} eV$ and the axion-photon coupling constant $g_{a\gamma} \sim 4.4 \cdot 10^{-11} GeV^{-1}$, obtained in [10] based coronal heating problem solution by means of axion origin photons and the Higgs ADM.

but unfortunately, no sooner than few years from now. In the meantime, we received the “experimental” data, which, oddly enough, are identical to the axions of dark matter on the Sun (see Eq. (4), the red star in Fig. 2, and Fig. 1 in [10]) and the additional component of the dark matter axions in our galactic halo (see Eq. (8)).

Below we try to explain how the “invisible” axions, being an insignificant part of DM, turn into axions of cold dark matter, which have almost no direct relation to the mysterious identity of dark matter in the Universe [43, 44], and thus, they are not a direct participant in the formation of halos of cold dark matter in galaxies. The main result is that the “invisible” axions of hot dark matter with high FSL (see left panel in Fig. 3) predetermine the formation of asymmetry of baryons during the inflation of the Universe, and consequently, the halo of asymmetric cold dark matter (CDM) with low FSL, which arises as a bound state of Higgs boson dark matter [45] (see [46, 47]). As of the period after inflation

(up to the present time), some remnants of the “invisible” axions turn into CDM, but almost without participation of the CDM axions in the ADM halo (see [10]).

From here, a difficult but intriguing question arises: How does the high density of “invisible” axions during the inflation of the Universe turn into low density of dark matter axions immediately after the inflation?

First, according to the remarkable work by Co & Harigaya [33], we use a mechanism called axiogenesis, in which the cosmological excess of baryons over antibaryons is generated from the rotation of QCD axion. This is because the PQ symmetry is an approximate global symmetry, which is clearly broken by the QCD anomaly. Given that the symmetry is not exact (since quantum gravity does not allow global symmetry [48–52]), it is likely that the PQ symmetry is significantly broken in the early Universe and caused the rotation of the axion.

In other words, as soon as the QCD scale becomes small enough, the axion begins to rotate, and the kinetic energy of rotation becomes greater than the barrier of the axion’s cosine potential (see Fig. 3). As a result, the number of axions increases [33], thus generating a high density of “invisible” axions in the inflationary Universe (see e.g. [53]).

But the most remarkable fact is that the kinetic energy of rotation, which becomes greater than the potential barrier of the axion, transforms into a large number of axions, and due to the kinetic energy of the axion field, these axions pass into other fields and generate particles that appear in the form of baryons and leptons (see left panel in Fig. 3), and especially the asymmetric dark matter (right panel in Fig. 3) appearing from the compound DM Higgs boson [46, 47]. When the kinetic energy of rotation falls below the axion potential, a large number of “invisible” axions practically disappear due to the production of baryons and leptons, and the remaining axion “marble” settles down to the minimum point, generating low-density axion CDM. At the same time, the cold ADM with a mass of ~ 5 GeV (see Fig. 6 in [36]) forms a halo of cold ADM with a high density in the post-inflation Universe and till nowadays.

From here we understand that at high temperatures the kinetic energy of rotation exceeds the height of the axion potential (see Fig. 3), and this means that a high density of “invisible” axions, or more precisely, the hot DM axions, appears in the inflationary Universe, when the kinetic energy the axion field flows into the other fields and generates particles. In other words, on the one hand, the rotation of the axion effectively transforms into quarks and the asymmetry of matter and antimatter. On the other hand, the greater the asymmetry of matter, the lower is the density of “invisible” axions immediately after the inflation. When the kinetic energy of rotation becomes lower than the height of the axion potential, i.e. at low temperatures of the axion potential (see Fig. 3), the axion marble settles and oscillates around this minimum, generating axion CDM with low density (in contrast to

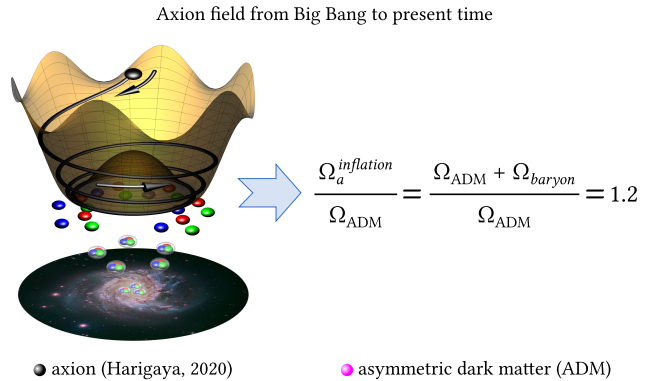


FIG. 3. Sombrero-like potential of the Peccei-Quinn field at temperatures above (below) the critical temperature of the QCD phase transition. At high temperatures, when the kinetic energy of rotation, exceeding the height of axion potential (left panel from [54]), generates a high concentration of “invisible” axions, or more precisely, the hot axion DM in the inflation, and, as a result, the kinetic energy of the axion field flows into other fields and generates particles. At low temperatures of the axion potential, when the axion “marble” settles, it will revolve around this minimum (left panel from [54]), generating axion cold dark matter. This is the result of the formation of post-inflation in the Universe. Note that the kinetic rotation exceeding the height of the axion potential, not only produces an asymmetry of baryons and leptons (see the left panel – the formation of electrons, quarks and nucleons etc.) [33, 55], but also induces the charge asymmetry for the Higgs boson dark matter (see [46, 47]), with a rather large mass of ~ 5 GeV (see Fig. 6 in [36]), which at the same time forms the halo of cold Higgs ADM (right panel).

the hot DM axions).

In this regard, according to [33], we find that the axions abundance during the Universe inflation (see left panel in Fig. 3)

$$\frac{\Omega_a}{\Omega_{DM}} \approx 140 \left(\frac{f_a}{10^8 \text{ GeV}} \right) \left(\frac{130 \text{ GeV}}{T_{WS}} \right)^2 \left(\frac{0.1}{c_B} \right) \sim 1.2, \quad (3)$$

is much higher than the observed Ω_{DM} abundance for $f_a = O(10^6) \text{ GeV}$ (and $c_B \sim 0.117$) which satisfies the astrophysical constraints [56].

Although it matches well with $\Omega_a/\Omega_{DM} \sim 1.2$ [33], it is still “a little” wrong. First, because the use of $f_a = O(10^6) \text{ GeV}$ (Eq. (3)) must be replaced with the energy scale value $f_a \sim 2 \cdot 10^8 \text{ GeV}$ (see Eq. (4)), which determines the values of the hadronic axion-photon coupling and the mass m_a (see Fig. 2 and Fig. 1 in [10]):

$$g_{a\gamma} \sim 4.4 \cdot 10^{-11} \text{ GeV}^{-1}, \quad m_a \sim 3.2 \cdot 10^{-2} \text{ eV}, \quad (4)$$

The latter, surprisingly enough, are the “experimental” key to the existence of cold dark matter axions (see Eq. (8)) – this is a direct proof of the solution to the problem of solar corona heating, which is associated with the

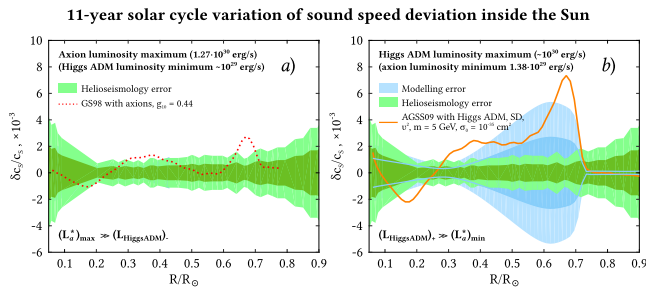


FIG. 4. Deviation of the radial speed of sound profile (Sun - model)/Sun in the solar interior from values obtained for two models: (a) the red dots from the values [58] with axions almost coincide with the values in [59] and (b) the asymmetric Higgs dark matter captured inside the Sun (solid orange line of ADM [36]). Colored areas indicate 1σ and 2σ errors in modeling (thick blue bar; [60, 61]) and helioseismological inverses (thinner green bar; [62, 63]). The deviation of the radial speed of sound is associated with the part of the corona luminosity [10] in the total luminosity of the Sun, which can be easily determined from (a) the solar maximum (involving the maximum axion luminosity fraction $((L_a^*)_{max} \gg (L_{HiggsADM})_-)$ and (b) the solar minimum (involving minimum fraction of the axion luminosity $((L_a^*)_{min} \ll (L_{HiggsADM})_+)$ and is in good agreement with nonstandard solar model.

hot dark matter axions on the Sun and the ADM halo in solar neighborhood [57] and which, unlike axions, is anti-correlated (through vertical density waves from the disk to the Sun) with 11-year S-stars around the black hole (see Fig. 4 and Eqs. (27)-(28) in [10]). Second, let us remind that the most fundamental problem of the Standard Model is the appearance of the scalar component of the two-particle gauge field in a form of the Higgs boson dark matter. According to Eqs. (18)-(44) in [46], this part also has nonzero vacuum value, which appears as a result of spontaneous breaking of symmetry [47]. So it is natural to consider such field as the Higgs field, scalar with respect to interior indices. At the same time, such scalar field contributes into the gravitational field through the energy-momentum tensor. Thus, the Higgs bosons, scalar with respect to interior indices, may be considered a candidate for a component of dark matter (see Fig. 4)!

So what is so special about this Higgs dark matter particle? We know that the existence of dark matter in the Universe is a striking evidence that physics goes beyond the Standard Model, although its nature remains a mystery. At the same time, the closeness of the energy densities of DM and baryons $\Omega_{DM} \approx 5.3\Omega_{baryon}$ [64, 65] motivates the idea of asymmetric dark matter (ADM) [66–74], based on the assumption that the current DM density is determined by the η_{DM} asymmetry in the DM sector, similar to the baryon asymmetry η_{baryon} . Then

$$\frac{\Omega_{DM}}{\Omega_{baryon}} = \frac{m_{DM}}{m_N} \frac{\eta_{DM}}{\eta_{baryon}} \quad (5)$$

where m_{DM} is the DM mass and m_N is the nucleon mass. If two asymmetries are generated by the same mechanism, or one dark asymmetry is responsible for the other – baryon asymmetry arising from leptogenesis, we expect $\eta_{DM} \sim \eta_B$. Hence it follows that taking the value $m_{DM} = m_{HiggsADM} \sim 5 \text{ GeV}$ and $m_N \approx 0.939 \text{ GeV}$, one can obtain the value

$$\frac{\Omega_{DM}}{\Omega_{baryon}} = \frac{m_{DM}}{m_N} \frac{\eta_{DM}}{\eta_{baryon}} \approx \frac{m_{HiggsADM}}{m_N} \approx 5.32, \quad (6)$$

which suggests that, according to Co & Harigaya [33], the Eq. (3) (see left panel in Fig. 3) coincides with the high density of “invisible” hot dark matter axions during the Universe inflation (see right panel in Fig. 3).

$$\begin{aligned} \frac{\Omega_a^{inflation}}{\Omega_{HiggsADM}} &\approx \frac{\Omega_{HiggsADM} + \Omega_{baryon}}{\Omega_{HiggsADM}} \approx \\ \frac{\Omega_{HiggsADM} + \Omega_{HiggsADM}/5.32}{\Omega_{HiggsADM}} &\approx 1.2, \end{aligned} \quad (7)$$

where the new physics manifests not only Eq. (7) (see right panel in Fig. 3), but also a description of the low density of cold dark matter axions in the post-inflation Universe (see Eq. (17) in [75])

$$\Omega_a^{post-inflation} \approx \left(\frac{6 \mu eV}{m_a} \right)^{7/6} \approx 4.5 \cdot 10^{-5}, \quad (8)$$

which, on the basis of “experimental” data, identically coincides with the values of the hadronic axion-photon coupling $g_{a\gamma}$ and the mass m_a on the Sun (see Eq. (4), Fig. 2 and Fig. 1 in [10]). This means that axions of hot dark matter on the Sun and axions of cold dark matter in our galactic Higgs ADM halo (see Eq. (8)) are absolutely identical!

Most importantly, this means that the same axions can be the hot dark matter, e.g. on the Sun, or the axions of CDM in the Galaxy, although the axion component is very insignificant (see Eq. (8)) in the ADM halo [10]. As a consequence, the flux of hot dark matter axions with high FSL, emitted from the core through the surface of the Sun, can scatter across the galaxy without high FSL, and surprisingly, with time, indently coinciding with the axions of CDM in the ADM halo from the center to the edge of the galaxy.

But the most remarkable fact is that our data on the axions dark matter in the form of the estimates of the hadronic axion-photon coupling $g_{a\gamma}$, the mass m_a and the ADM mass, experimentally coincide, according to [10], with the solution for the Higgs ADM chronometer in the S-stars interior, which controls the solar cycles of the dark matter axions luminosity, and consequently, is the remarkable solution for the problem of solar corona heating using photons of axion origin and Higgs ADM – a complete proof of the existence of the Higgs ADM.

And, finally, the fundamental results in both directions make it possible to obtain (through indirect detection) the convincing evidence of the existence and nature of the Higgs asymmetric dark matter halo (see post-inflation dark matter in the Universe) near a black hole and, as a result, in the solar neighborhood.

Taking into account the above remarks, we arranged our paper in the following way. In Section II we discuss the effect of virtually empty magnetic tubes and dark matter axions in the Sun’s core. In Section II A we present the convective heating and floating of magnetic tubes – the phenomenon of solar dark matter axions. In Section II B we discuss the physics of magnetic reconnection of the magnetic tubes in the lower layers and the observed features of the slope of Joy’s law. Finally, in Section III we provide a summary and perspective of this work.

II. EFFECT OF VIRTUALLY EMPTY MAGNETIC FLUX TUBES AND SOLAR AXION IN THE SUN INTERIOR

The appearance of sunspots on the solar surface is one of the major manifestations of solar activity demonstrating the cyclic behavior with the period of about 11 years (see e.g. [76]). A very high density of the magnetic field is observed within the sunspots, which suppresses the convective heat flow from the solar interior to the surface [2, 3, 5, 77]. That is why the sunspots are cooler and darker against the background of the solar disk. More than a hundred years ago [78] discovered the vertical “vortices” of the magnetic field in the sunspots. About a year later British astronomer [79] was conducting the observations in Kodaikanal (Tamil Nadu, India) and found that in spite of the Hale’s vertical “vortices”, the magnetic field in the penumbra is radially divergent from the center of a sunspot. The mechanism of the sunspot formation including the umbra and penumbra as well as the Evershed effect are still the subject of active discussions and studies today, and lots of fundamental questions remain unanswered [80–83]. We consider some possible solutions to these problems below.

We are mostly interested in effects for which the current theories, assuming that the sunspots are produced by the dynamo action at the bottom of the convection zone, fail to provide the convincing proofs and explain the dynamo action in the convection zone. This problem becomes even stronger with the recent findings. The numerical simulations of the solar dynamo have not revealed thin MFTs of the comparable strength so far (see e.g. [84–86]). The helioseismology does not give any evidence of the upward MFTs existence either [87, 88]. This is especially important because of the recent helioseismological investigations which set the strict limitations on the velocities of large-scale convection inside the Sun and demonstrated the inconsistency with the existing global magnetoconvection e.g. [89] modeling [87, 88, 90–93].

Thus, our major question is: “How are the sunspots generated by the strong magnetic field at the base of the convection zone without any dynamo action?”, or otherwise “Which fundamental processes connect the sunspot cycle with the large-scale magnetic field of the Sun?”. Or even more precisely, “What are the fundamental processes, associated with solar axions, connect the sunspot cycle to the large-scale magnetic field of the Sun?”

Of all the known concepts playing a noticeable role in understanding of the link between the energy transfer and the darkness of sunspots, let us consider the most significant one, in our opinion. It is based on the Parker-Biermann cooling effect [2–4] in strong fields, which explains how the suppression of the Parker’s convective heat transport in the lower part of the magnetic tube manifests itself.

In order to understand the physics of the Parker’s suppression of the convective heat transport in strong magnetic fields, we need to turn to the dark matter axions, born in the core of the Sun. With solar axions and the existence of a magnetic O-loop inside the MFT near the tachocline, the answer becomes very simple. When a magnetic O-loop is formed inside the MFT near the tachocline through the Kolmogorov turbulent cascade (see Fig. 2), the high-energy photons from the radiation zone experience the axion-photon oscillations in this O-loop, and the so-called axions of photonic origin appear under the sunspot. This means that the cooling effect of Parker-Biermann exists due to the disappearance of barometric equilibrium [6] and, as a consequence, the manifestation of the photon free path (Rosseland length; see Fig. B.3 in [10]) from the tachocline to the photosphere, which is confirmed by axions of photonic origin after photon-axion oscillations in the O-loop (see Fig. 5).

On the other hand, a certain stream of high-energy photons coming from the radiation zone through the tachocline and through the “ring” (between the magnetic wall of the flux tube and the O-loop) (see Figs. 5 and 6) allows to use the barometric equilibrium [6], i.e. no Parker-Biermann cooling effect, to determine the convective heating $(dQ/dt)_2$ (see Sect. II A).

This solution explicitly depends on the lifetime of the magnetic tubes rising from the tachocline to the solar surface. Therefore, because of the magnetic reconnection in the lower layers (see Fig. 4 in [98]), it is not the final stage of the simulation. The essence of a virtually empty tube which is first born without a dynamo of any kind (Fig. 7a), is related to the physics of the turbulent reconnection of magnetic bipolar structures (see Fig. 7b,c and Eq. (8) in [99]). It is therefore connected to a very rare model of fluctuation dynamo caused by a multiscale turbulence model (see [100]), but necessarily through the so-called turbulent reconnection [101–103]. In this case the turbulent pumping of the plasma from the azimuthal field is repeated in the Ω -loop again and again (Fig. 7).

As described by [98, 104–106], the upward convection flow around the rising Ω -loop brings its “legs” together in such a way that the magnetic field reconnection oc-

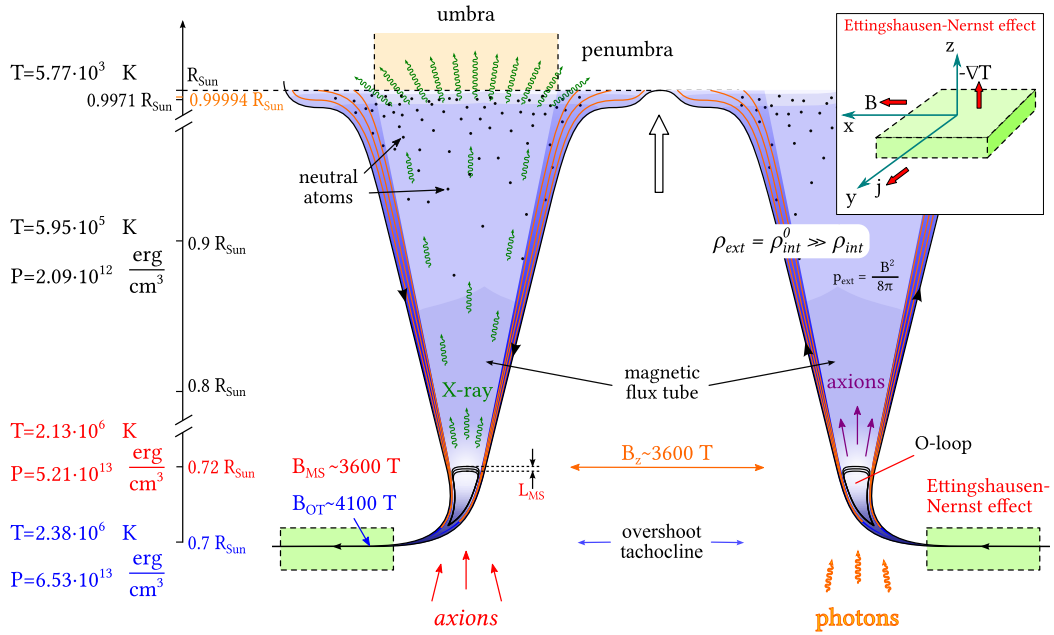


FIG. 5. Topological effects of magnetic reconnection inside the magnetic tubes with the “magnetic steps” (Fig. B.1 in [10]). The left panel shows the temperature and pressure change along the radius of the Sun from the tachocline to the photosphere [94], L_{MS} is the height of the magnetic shear steps. At $R \sim 0.72 R_{Sun}$ the vertical magnetic field, which is developed from the horizontal magnetic field through the well-known Kolmogorov turbulent cascade (see Fig. 6), reaches $B_z \sim 3600$ T, and the magnetic pressure $p_{ext} = B^2/8\pi \simeq 5.21 \cdot 10^{13} \text{ erg/cm}^3$ [94]. The very cool regions along the entire convective zone caused by the Parker-Biermann cooling effect have the virtually zero internal gas pressure, i.e. the maximum magnetic pressure in the magnetic tubes.

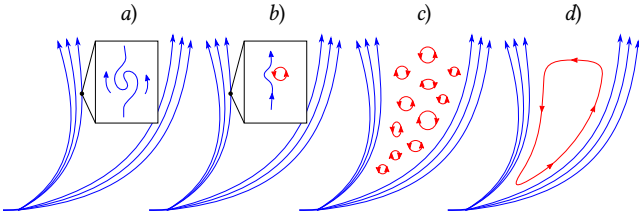


FIG. 6. Kolmogorov turbulent cascade [95–97] and magnetic reconnection in the lower layers inside the unipolar magnetic tube (Fig. B.2 in [10]). Common to these various turbulent systems is the presence of the inertial range of Kolmogorov, through which the energy is cascaded from large to small scales, where dissipative mechanisms (as a consequence of magnetic reconnection) overcome the turbulent energy in plasma heating.

curs across this loop. This cuts off the loop from the azimuthal magnetic field, turning it into an O-loop (see Fig. 3 in [104] and Fig. 4 in [98]). After that the azimuthal magnetic field restores its initial configuration and becomes ready for another process with Ω -loop.

Let us now make some important remarks on the turbulent reconnection, the Ω -loop transformation into the

O-loop by rapid “legs” closure, the restoration of the initial azimuthal field and the preconditions for another Ω -loop formation in the same place. It is also necessary to explain the physical interpretation of the overshoot process near the tachocline and estimate the velocity v_{rise} and time τ_{rise} of the magnetic tube rise from the overshoot boundary layer – starting with the azimuthal magnetic flux strength of $B_{tach} \sim 4 \cdot 10^7 \text{ G}$ (see Eq. A.17 in [10]).

One ultimate goal of this section is to determine the general regularities in the theory of MFTs, which are generated by the magnetic buoyancy of virtually empty tubes rising from the tachocline to the surface of the Sun (Fig. 5). Another one is the physical interpretation of the process of MFTs reconnection in the lower layers of the convection zone (Fig. 7). Not only this is related to the magnetic cycles of flux tubes coinciding with the observed Joy’s law for the tilt angle, but both effects (surprisingly enough) are induced by the existence of DM – the solar axions generated in the core of the Sun.

Magnetic reconnection in the lower layers

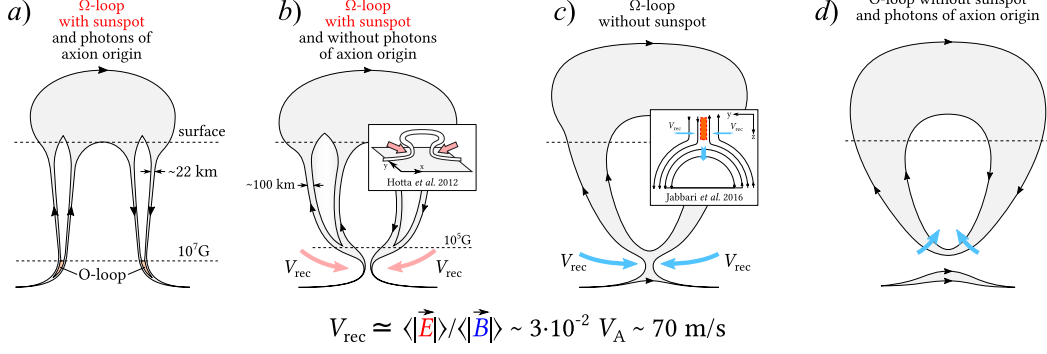


FIG. 7. A sketch of the magnetic reconnection near the tachocline. **(a)** Ω -loop forms the sunspot umbra (with photons of axion origin from the O-loops) via the indirect thermomagnetic EN effect but without reconnection (Fig. 5); **(b)** Ω -loop with a sunspot (without photons of axion origin and O-loops); pink arrows show the upward convective flow between the “legs” of the Ω -loop during its rise from the tachocline to the visible surface; **(c)** Ω -loop with reconnection and without a sunspot; **(d)** O-loop without a sunspot. Going through the stages (a), (b), (c), (d) (left to right), the convection around the rising Ω -loop “closes” it at its base, then a free O-loop is formed via reconnection (d), and the initial configuration of the azimuthal field at the bottom of this region is restored. Blue arrows show the substance motion leading to the loop “legs” connection.

A. Convective heating and the buoyant rise of magnetic flux tubes: the phenomenon of solar dark matter axions

The first problem is devoted to the study of the effect of virtually empty magnetic tubes and the phenomenon of solar dark matter axions.

The assumption that the virtually empty magnetic tubes (Fig. 5) are neutrally buoyant ($\rho_{\text{int}} = \rho_{\text{ext}}$ [107]) implies that the temperature inside these tubes is lower than that of the ambient medium (Fig. 5 and Fig. 7a). This leads to the heat inflow, and consequently, the flux tube rises up (see [108] or Sect. 8.8 in [109]). For a horizontal tube with a cross-section of radius a the rise velocity follows from the Parker’s analysis (see [108], Eq. (60) in [110]):

$$v_{\text{rise}} = 2 \frac{H_p}{\tau_d} \frac{B^2}{8\pi p_{\text{ext}}} \left(-\delta + 0.12 \frac{B^2}{8\pi p_{\text{ext}}} \right)^{-1}, \quad (9)$$

where $H_p = \Re T_{\text{ext}}/g = p_{\text{ext}}/g\rho_{\text{ext}} = 0.08 R_{\text{Sun}}$ [111–113] is the pressure scale height at the tachocline, T_{ext} and p_{ext} are the external gas temperature and pressure, $\delta \equiv Y = \nabla_e - \nabla_{\text{ad}} = -c_p^{-1} dS/d\xi = -c_p^{-1} H_p dS/dz$ is the dimensionless entropy gradient (see [110, 114, 115]), $\nabla_e \equiv d \ln T_{\text{ext}}/d \ln p_{\text{ext}}$ and $\nabla_{\text{ad}} \equiv (\partial \ln T/\partial \ln p)_s$ are the local and adiabatic temperature gradients in external and internal plasma [110, 116, 117], s is the specific entropy, c_p is the heat capacity at constant pressure, and τ_d is the radiation and/or convection diffusion time of the flux tube:

$$\tau_d = \frac{c_p \rho a^2}{k_e} \simeq c_p \rho a^2 \left[\frac{c_p F_{\text{tot}}}{g} \left(1 + \frac{2\ell_{\text{ov}}}{5H_p} \right)^\nu \right]^{-1}. \quad (10)$$

where for the fully ionized gas $c_p = 2.5\Re$ (\Re is the gas constant in the ideal gas law $p = \rho\Re T$), $T(z)$ and $\rho(z)$ are the mean temperature and density; k_e is the radiative heat conductivity (see Eq. (36) in [110]); $\ell_{\text{ov}} \approx 0.37 H_p$ [110, 118] is the thickness of the overshoot layer; the total radiative energy flux $F_{\text{tot}} = L/(4\pi r^2)$ depends on the Sun luminosity L ; g is the gravitational acceleration.

Next we apply the condition of hydrostatic equilibrium, $dp/dz = \rho g$, when the adiabatic temperature gradient $(dT/dz)_{\text{ad}} = g/c_p$ may be used, and the neutral buoyancy of the flux tube in the overshoot zone $(|\delta T|/T_{\text{ext}})^{-1} \sim \beta \equiv 8\pi p_{\text{ext}}/B^2$. This way we are able to estimate the time of the radiative and/or convective diffusion τ_d (see Eq. (10)) of the flux tube:

$$\tau_d = \frac{c_p \rho a^2}{k_e} \approx |\delta T| c_p \rho \frac{a^2}{(1.148)^\nu \delta z F_{\text{tot}}}, \quad (11)$$

where

$$\delta z \sim (1.148)^{-\nu} \left(\frac{a}{H_p} \right)^2 H_p \frac{\nabla_e}{\nabla_{\text{rad}}}, \quad \text{where } \nu \geq 3.5, \quad (12)$$

$$F_{\text{tot}} = \frac{L}{4\pi R_{\text{tachoc}}^2} = H_p \frac{\nabla_{\text{rad}}}{\nabla_e} \left(\frac{dQ}{dt} \right)_1. \quad (13)$$

Here $\nabla_{\text{rad}} = (\partial \ln T_{\text{ext}}/\partial \ln p_{\text{ext}})_{\text{rad}}$ is the radiative equilibrium temperature gradient; $(dQ/dt)_1$ is the rate of radiative heating, which only depends on the thermodynamic parameters k_e and T_{ext} of the ambient plasma, depending only on the radial distance from the Sun center [110, 116].

As a result, it is not difficult to show that the van Ballegooijen model combining equations (9)-(13) gives the final expression for the rise time by radiation and/or convective diffusion from the boundary layer of the overshoot to the solar surface,

$$\tau_d \approx \frac{2}{\beta} T_{ext} \left[\frac{1}{c_p \rho_{ext}} \left(\frac{dQ}{dt} \right)_1 \right]^{-1}, \quad (14)$$

and the lifting speed of the MFT from the overshoot boundary layer to the surface of the Sun,

$$v_{rise} = H_p \nabla_{ad} \frac{1}{p_{ext}} \left(\frac{dQ}{dt} \right)_1 \left(-\delta + 0.12 \frac{B^2}{8\pi p_{ext}} \right)^{-1}, \quad (15)$$

$$\nabla_{ad} = \nabla_e \simeq 0.4,$$

which are almost identical to the equations (29) and (30) of [119].

Hence, we understand that the van Ballegooijen model is a special case for magnetic fields of $B_{tach} \leq 10^5 G$, under which a magnetic dynamo can exist. On the other hand, we know that based on the holographic BL mechanism, generating (in contrast to dynamo!) the toroidal magnetic field in the tachocline, the universal model of flux tubes predetermines the existence of not only the fields of $B_{tach} \leq 10^5 G$, but also the strong magnetic fields of the order $B_{tach} \sim 10^7 G$.

Unlike the special van Ballegooijen model, we adopt the universal model of MFTs with

$$v_{rise} = 2 \frac{H_p}{\tau_d} \frac{B^2}{8\pi p_{ext}} \left(-\delta + 0.12 \frac{B^2}{8\pi p_{ext}} \right)^{-1},$$

where

$$\tau_d = \frac{c_p \rho a^2}{k_e} \left[1 + \left(\frac{dQ}{dt} \right)_2 / \left(\frac{dQ}{dt} \right)_1 \right]^{-1}. \quad (16)$$

Here $(dQ/dt)_2$ represents the radiative diffusion across the flux tube due to the temperature difference ($\delta T \equiv T - T_{ext}$) between the tube and the external plasma (see [119]).

Using simple calculations of equations (9) and (16) for MFTs, it is easy to show that with the help of the total expression

$$\frac{dQ}{dt} = \left(\frac{dQ}{dt} \right)_1 + \left(\frac{dQ}{dt} \right)_2 \quad (17)$$

of the universal model

$$\tau_d \approx \frac{2}{\beta} T_{ext} \left[\frac{1}{c_p \rho_{ext}} \frac{dQ}{dt} \right]^{-1} \quad (18)$$

and

$$v_{rise} = H_p \nabla_{ad} \frac{1}{p_{ext}} \frac{dQ}{dt} \left(-\delta + 0.12 \frac{B^2}{8\pi p_{ext}} \right)^{-1},$$

$$\nabla_{ad} = \nabla_e \simeq 0.4, \quad (19)$$

which is the general case of the so-called universal model of van Ballegooijen-Fan-Fisher (vanBFF model).

On the other hand, let us remind that on the basis of the BL holographic mechanism, generating the toroidal magnetic field in the tachocline, the universal model of flux tubes is predetermined by the existence of strong magnetic fields of the order of $B_{tach} \sim 10^7 G$. Since the physics of the holographic BL mechanism does not involve a magnetic dynamo, we often refer to it as the universal antidynamo vanBFF model. It is determined by the following total energy rate per unit volume:

$$\frac{dQ}{dt} = \left(\frac{dQ}{dt} \right)_1 + \left(\frac{dQ}{dt} \right)_2 = \left(\frac{dQ}{dt} \right)_1 \left[1 + \frac{\alpha_1^2}{\nabla_e} \left(\frac{H_p}{a} \right)^2 \frac{1}{\beta} \right], \quad (20)$$

where

$$\left(\frac{dQ}{dt} \right)_1 = -\nabla \vec{F}_{rad} = F_{tot} \frac{\nabla_e}{\nabla_{rad}} \frac{1}{H_p} = k_e \nabla_e \frac{T_{ext}}{H_p^2}, \quad (21)$$

$$\left(\frac{dQ}{dt} \right)_2 = -k_e \frac{\alpha_1^2}{a^2} (T - T_{ext}), \quad (22)$$

where we used the approximate relation $|\delta T|/T_{ext} \sim 1/\beta$; the parameter $\alpha_1^2 \approx 5.76$ [119, 120]; \vec{F}_{rad} is the radiative energy flux [116]; $\nabla_e \sim 1.287 \nabla_{rad}$ (see Table 2 in [116]); H_p/a is a factor for the lower convection zone (see [110]).

As a result, we understand that the heating rate of MFTs consists of the rate of radiative and convective heating (see Eqs. (17)-(22); Eq. (10) in [119] and Eq. (7) in [120]):

$$\frac{dQ}{dt} = \rho T \frac{dS}{dt} \approx -\text{div} \vec{F}_{rad} - k_e \frac{\alpha_1^2}{a^2} (T - T_{ext}), \quad (23)$$

where S is the entropy per unit mass. The first term $(dQ/dt)_1$ determines the mean temperature gradient between the lower convection zone and the overshoot (see Eq. (21)). It deviates from the radiative equilibrium substantially, implying the existence of the nonzero divergence of the heating radiation flux. The second term $(dQ/dt)_2$ (see Eq. (22)) represents the radiation diffusion through the flux tube because of the temperature difference between the tube and the external plasma. Its effect is to reduce the temperature difference.

Hence, it is clear that with strong toroidal magnetic fields in the tachocline (of the order $> 10^5 G$) the second term $(dQ/dt)_2$ (in contrast to [110, 119-121]) is the

dominant source of convective heating. For the toroidal magnetic field $B_{tach_o} \sim 4 \cdot 10^7 G$ in the tachocline, our estimate of the second term

$$\left(\frac{dQ}{dt}\right)_2 = \frac{\alpha_1^2}{\nabla_e \beta} \frac{1}{\left(\frac{H_p}{a}\right)^2} \left(\frac{dQ}{dt}\right)_1 \geq 5 \cdot 10^4 \text{ erg} \cdot \text{cm}^{-3} \text{s}^{-1} \quad \text{at } \beta \simeq 1 \quad (24)$$

is related to the first term $(dQ/dt)_1 \approx 29.7 \text{ erg} \cdot \text{cm}^{-3} \cdot \text{s}^{-1}$ (see Eq. (18) in [119]) and the following parameters: $\alpha_1^2 \approx 5.76$ [119, 120], $\nabla_e \approx 0.4$ (see Table 2 in [116, 119]), $1/\beta = B_{tach_o}^2/8\pi p_{ext} = 1$, $\nabla_e/\nabla_{rad} \approx 1.287$, $a = (\Phi/\pi B_{tach_o})^{1/2} \leq 0.1 H_p$ (see [122]) with an average value of magnetic flux $\Phi \sim 10^{21} Mx$ (see e.g. [123]).

Taking into account the consequences of the non-local theory of mixing length [107, 116], it can be shown that thin, neutrally buoyant flux tubes are stable in the stably stratified medium, provided that its field strength B is smaller than a critical value B_c [110], which is approximately given by

$$\frac{B_c^2}{8\pi p_{ext}} = -\gamma\delta = -\frac{5}{3}\delta. \quad (25)$$

So, for the maximum value of the toroidal magnetic field ($B_{tach_o} \sim 4 \cdot 10^7 G$) the estimate of the rise time of the radiation and/or convection diffusion of the flux tube (see Eq. (18))

$$\tau_d \approx \frac{2}{\beta} T_{ext} \left[\frac{1}{c_p \rho_{ext}} \left(\frac{dQ}{dt}\right)_2 \right]^{-1} \geq 10^4 \text{ year} \quad (26)$$

and the lifting speed of an almost empty magnetic tube (see Eqs. (24), (25))

$$v_{rise} \simeq \frac{H_p \nabla_e}{p_{ext}} \left(\frac{dQ}{dt}\right)_2 \frac{1}{0.72} \leq 10^{-8} \text{ km/s} \quad (27)$$

show that the existence of MFTs on the surface of the Sun is meaningless.

In this regard, there is one more beautiful task associated with our problem of almost total suppression of radiative heating in virtually empty magnetic tubes (see Fig. 5). Let us remind that photons going from the radiation zone through the horizontal field of the O-loop near the tachocline (Fig. 5) are turned into axions, thus almost completely eliminating the radiative heating in the virtually empty magnetic tube. Some small photon flux can still pass through the “ring” between the O-loop and the tube walls (see Fig. 5) and reach the penumbra. Let us denote the area of the magnetic tube “ring” by $2\pi r a_{conv}$, where r is the magnetic tube radius, and a_{conv} is the width of the “ring”.

What is the physics behind the appearance of the “ring” between the O-loop and the walls of the magnetic tube (Fig. 8)? In simple words, one can say the

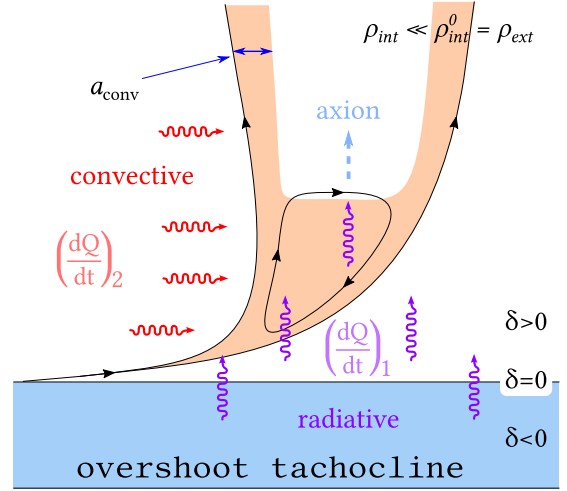


FIG. 8. A sketch of the magnetic tube born anchored to the tachocline and risen to the solar surface by the neutral buoyancy ($\rho_{ext} = \rho_{int}^0$). The strong convection suppression inside the tube leads to the abrupt decrease of temperature and density ($\rho_{int}^0 \gg \rho_{int}$), which in its turn leads to the significant decrease in gas pressure in the umbra. At the top of the overshoot tachocline the first term $(dQ/dt)_1$ characterizes the radiative heating which depends on the thermodynamic quantities k_e and T_{ext} of the external plasma, changing with the distance from the center of the Sun only (see Eq. (21)). The second term $(dQ/dt)_2$ represents the diffuse radiation (by convective heating) through the flux tube because of the temperature difference between the tube and the ambient plasma (see Eq. (22)). The keV photons (see Fig. 2 in [124]) coming from the radiation zone are turned into axions in the horizontal magnetic field of the O-loop (see Fig. 5). Therefore, the radiative heating almost vanishes in the virtually empty magnetic tube. The base of the convection zone is defined as a radius at which the stratification switches from almost adiabatic ($\delta = \nabla_e - \nabla_{ad} = 0$) to sub-adiabatic ($\delta = \nabla_e - \nabla_{ad} < 0$). Meanwhile, the external plasma turns from sub-adiabatic to super-adiabatic ($\delta = \nabla_e - \nabla_{ad} > 0$).

following. The appearance of the “ring” cross-section is the result of the production of both axion-origin photons (by converting solar axions into photons in the tachocline) and photon-origin axions (through the conversion of high-energy photons from the radiation zone to axions in the tachocline). From here, on the one hand, the axions of photonic origin are the part of the manifestation of the mean free path of axion origin photons from the tachocline to the photosphere. On the other hand, they are the part of the manifestation of magnetic tube “ring”, where the convective heating $(dQ/dt)_2$ dominates over the radiative heating $(dQ/dt)_1$.

As a result, assuming the mean width of the “ring”

$$a_{conv} \sim 3.7 \cdot 10^{-4} H_p, \quad (28)$$

we apply a new analysis of the universal vanBFF model (see Eq. (19) and (17) (analogous to [110]) or (19) and

(25) (analogous to Eq. (29) in [119]), where the calculated values such as the magnetic flux Φ and the rise speed $(v_{rise})_{conv}$ of the MFT to the surface of the Sun, do not contradict the known observational data:

- the value of the magnetic flux of the tube (for $r \sim 70 \text{ km}$)

$$\Phi = 2\pi r a_{conv} B_{tach} \approx 3.7 \cdot 10^{21} \text{ Mx}, \quad (29)$$

which is in good agreement with the observational data of [123];

- the time of radiation diffusion of the flux tube (18)-(20)

$$(\tau_d)_{conv} = 2T_{ext} \left\{ \frac{1}{c_p \rho_{ext}} \left(\frac{dQ}{dt} \right)_1 \left[1 + \frac{\alpha_1^2}{\nabla_e} \left(\frac{H_p}{a_{conv}} \right)^2 \right] \right\}^{-1} \\ \approx 1.1 \cdot 10^5 \text{ s} \sim 1.3 \text{ day} \quad (30)$$

and, as a consequence, the magnitude of the lifting speed of the MFT (see Eq. (9))

$$(v_{rise})_{conv} = \frac{2.77 H_p}{(\tau_d)_{conv}} \sim 1.4 \text{ km/s}, \quad (31)$$

which are almost identical to the observational data of the known works by [125–127] and [128].

In this context, it is known that [125–127] and [128] recently detected significant magnetic perturbations at a depth of about 42-75 Mm (i.e. $\sim 0.9 R_{Sun}$) and showed that these perturbations were associated with magnetic structures that emerged with an average speed of 0.3-1.4 km/s and appeared at the surface several hours – 2 days after the detection of the perturbations. Interestingly, the results of several attempts to detect emerging magnetic flux prior to its appearance in the photosphere can be compared to our theoretical estimates (30)-(31) and demonstrate a surprising agreement as regards the velocity and time of the magnetic tube rise.

Hence, a very important question arises as to how the values of the rise time and speed of the MFTs, which are predetermined by the width of the magnetic tube “ring” (see Eq. (28) and Fig. 8), do not contradict the observational data of the Joy’s law. If this is the case, under strong magnetic fields in the tachocline, which are generated by the holographic principle of quantum gravity (see Fig.C.1 in [10]), solar axions cause the appearance of a “ring” around a MFT. Photons of the near-surface radiation of the overshoot regions passing through the horizontal magnetic field of the O-loop (see Figs. 5 and 8) are converted into axions, thus completely suppressing the radiation heating $(dQ/dt)_1$ within the width of the magnetic tube “ring” (see (28)).

On the other hand, the most interesting point is that if the axions, which are born in the Sun core, are directly converted into X-rays near the tachocline, then the axion-photon oscillations predetermine the appearance of magnetic sunspot cycles (see Sect. 3.2 in [21]). This is due to the fact that, according to [10], the formation of sunspots and their cycles is a consequence of the anticorrelated 11-year cycles of ADM density modulation inside the Sun. The latter, in their turn, are a consequence of the 11-year ADM halo density modulation in the fundamental plane of the galactic center, which closely correlates with the density modulation of baryonic matter near the super-massive black hole. From here, it is easy to show (see [10]) the anticorrelation identity between the indicators of the ADM density modulation in the solar interior and the number of sunspots. Or equivalently, between the indicators of the solar axions (or photons of axion origin) modulations and the sunspot cycles!

It means that if the rising speed of the buoyant magnetic tube, which is determined by the values of the magnetic field $\sim 4.1 \cdot 10^7 \text{ G}$ and the “ring” width $\sim 3.7 \cdot 10^{-4} H_p$, causes the appearance of MFTs in the form of sunspots, then the parameters of the universal vanBFF model, such as the magnetic cycles, are almost identical to the observational data of the tilt angle of Joy’s law.

B. Secondary reconnection of magnetic tubes in lower layers and the observed features of the tilt angle of Joy’s Law

The problem is devoted to physics of the magnetic reconnection of a magnetic tube in the lower layers, which is associated with the so-called reconnecting dynamo and the observed features of the tilt angle of Joy’s law.

In contrast to the primary reconnection inside magnetic tubes near the tachocline, which generates the O-loops, thus participating in the formation of photons of axion origin, as well as the axions of photon origin, from the O-loop to the photosphere, here we are interested in the secondary magnetic reconnection, which, although does not depend on sunspot cycles, but is necessarily related to the process of sunspots liftoff from the surface of the Sun.

In Fig. 9 one can see the conditions for the secondary reconnection between the O-loop (green lines) and the unipolar part of the Ω -loop (blue lines) that can organize them in the lower layer (Fig. 9, left) or in the upper layer (Fig. 9, right), thereby showing the appearance of bipolar magnetic tubes in various versions (Fig. 9c,d and g,h).

Finally, let us note that we have two types of primary magnetic reconnection inside the Ω -loop near the tachocline, one of which is manifested by the existence of a free O-loop (red lines in Fig. 6, green lines in Figs. 9a and 9e), and the other one practically does not exist. In other words, magnetic reconnection inside the Ω -loop may or may not accidentally give birth to a free O-loop near the tachocline (see Fig. 6). This means that if a

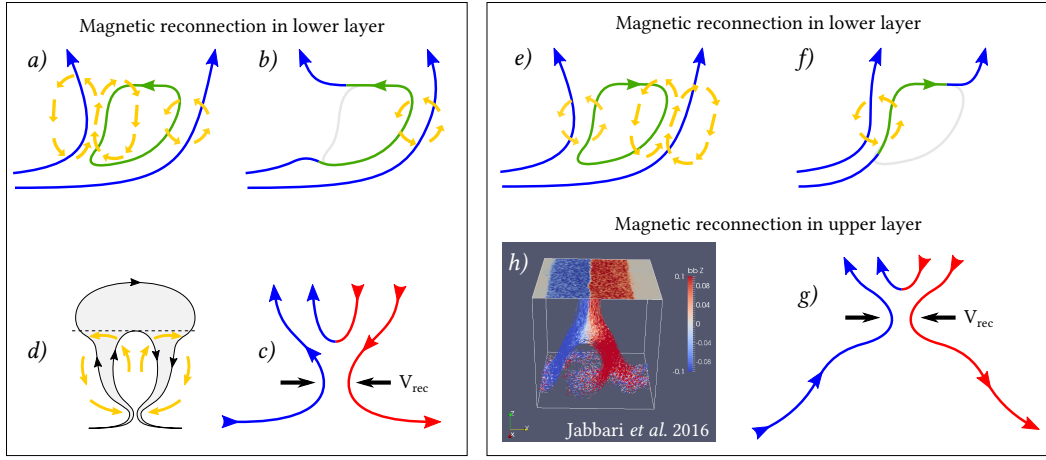


FIG. 9. Topological effects of magnetic reconnection in the lower (left) or upper (right) layers of the magnetic tube. Here, the unipolar part of the Ω -loop is rebuilt on its base, compressing the Ω -loop (blue lines) to form a free O-loop (green lines) (Fig. 7a). The yellow lines show the movement of the substance leading to the connection of the “leg” loop (see analogous Fig. 4 in [98]). If the O-loop (green lines) can randomly have different directions of magnetic fields, then the magnetic reconnection can generate loop “legs” in different layers, for example, in lower layers (Fig. 9c and also Fig. 9d as an analog of Fig. 7b) and upper layers (Fig. 9g and also Fig. 9h as an analog of Fig. 4 in [129]).

free O-loop is created in the Ω -loop near the tachocline via the primary reconnection, classical sunspots appear on the surface (see black tubes, Fig. 10), while the rare “transparent” bipolar tubes, not reaching the surface and having no O-loop inside, appear as “optically invisible” spots on the surface (see white bipolar tubes, Fig. 10).

Here arises a question: How does the secondary magnetic reconnection in the lower layers of flux tubes (with magnetic field strength $\sim 10^7 G$ (see Fig. 7a) and $\sim 10^5 G$ (see Fig. 7b), respectively) explain the physics and theoretical estimates of the buoyant tubes – the time and speed of the sunspot liftoff from the solar surface, and the tendency of the tilt angle of Joy’s law?

Let us first note the physics of primary reconnection in the lower layers of the magnetic flux tubes (with $B \sim 10^7 G$). Based on the mechanical equilibrium model (MEQ) of [131] and vanBFF MEQ model (see Sect. II A), we showed that the results of the simulation of flux tube trajectories without adiabatic ring flux drag in the super-adiabatic zone (see Fig. 8) are well represented in Fig. 11a,b (red lines). The most intriguing results of the simulation of flux tube trajectories are a very strong basis not only for understanding the complex physics, but also for understanding the theoretical estimates of buoyant MFTs, like the rise time and speed of rising to the Sun surface (see (30)-(31), and also analogous Fig. 1 and Fig. 5 in [132]), and the explanation of the tendency of the tilt angle of Joy’s law (see Fig. 11c,d), which do not contradict the known experimental data, for example, the well-known works of [133–142].

Further, we are interested in the second stage of modeling the trajectory of magnetic flux tubes (see Fig. 11), when a magnetic tube that reaches the solar surface

above the photosphere changes its shape and structure with the topological effect of the secondary magnetic reconnection in the lower layers of the magnetic tube, see Fig. 7b and 9a-c. Moreover, we believe that the secondary magnetic reconnection of the flux tubes leads to the real decrease in the magnetic field to $B \sim 10^5 G$ at $\sim 0.8 R_{Sun}$ (see Fig. 13), at which the evolution of the tubes (in thermal equilibrium (TEQ) with the surroundings it is often referred to as magnetic buoyancy [108]) is controlled by the latitudinal pressure gradient in magnetic layers on the overshoot tachocline that allows a balance between nonzero buoyancy force, curvature force and pressure force in the absence of azimuthal flow (see bottom panel in Fig. 2 in [146]; see also review and Fig. 5b in [147]), which generally allows a balance of TEQ between four main forces: nonzero buoyancy, magnetic tension, aerodynamic drag, and Coriolis force.

Despite our complicated theoretical calculations of the trajectories (Fig. 11a,b) of the flux tubes without drag of adiabatic flux ring in the superadiabatic convection zone (red lines: based on the MEQ model by [131] and the vanBFF MEQ model (see Sect. II A)) and involving the flux ring resistance in thermal equilibrium (blue lines: based on the TEQ model by [131]), below we will describe the scenario, which explains the simple physics of why the magnetic tubes emerging on the solar surface, can only be at low, and to a lesser extent at middle latitudes (see Figs. 11a,b and 12b).

The first part of the scenario consists in discussing the physics of magnetic flux buoyancy and, as a consequence, estimating the rise speed of an almost empty magnetic tube, v_{rise} , based on the vanBFF model (see Sect. II A), which simultaneously coincides with the known expres-

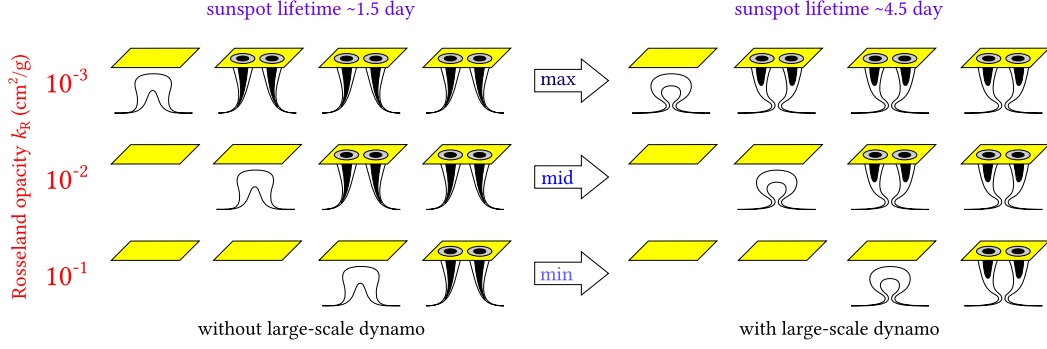


FIG. 10. The physical nature of the cycle of sunspots as a consequence of the modulation of MFTs, rising from the tachocline to the surface of the Sun. Left: “one” of the initial bipolar magnetic tubes is “invisible” due to the absence of a free O-loop and, thus, the absence of photons of axion origin in the Ω -loop, which, as a consequence, rises super-slowly to the solar surface: here the rise time of the magnetic tube from the boundary layer of the overshoot to the surface of the Sun is many orders of magnitude greater than the lifetime of the sunspot (see [80, 130] and vanBFF model (Sect. II A)). Right: simplifying the drawing, we drew different unipolar magnetic tubes that actually correspond to visible or “invisible” bipolar magnetic tubes, cyclically (from the maximum to the minimum of activity) appearing on the solar surface. The rough values of the Rosseland opacity k_R can be estimated using Eq. B.4 and Fig. B.1 in [10].

sions for the buoyancy speed, v_B (see e.g. [108]; see also Eq. (17) and Fig. 2 in [149]; Eq. (34) in [122]; Eq. (30) in [150]):

$$(v_{rise})_{conv} \equiv (v_B)_{conv} \approx v_A \left(\frac{\pi}{C_D} \frac{a_{conv}}{H_p} \frac{z}{H_p} \right)^{1/2}, \quad (32)$$

where $v_A \equiv B/(4\pi\rho_{int})^{1/2}$ is the Alfvén speed of the magnetic field (see e.g. [151]), $C_D \approx 1$ is the drag coefficient, ρ_{int} is the internal density of the gas in the MFT. It is assumed that the magnetic tube is formed inside the disk at an altitude $z/H_p \approx 1$.

For the neutral buoyancy condition ($\rho_{int} = \rho_{ext} \approx 0.2 \text{ g/cm}^3$; see Figs. 6 and 11 in [21, 152] and Fig. 5) and the strong toroidal field of the magnetic tube, $B_{tach}^{Sun} = 4.1 \cdot 10^7 \text{ G}$, as well as the average width of the “thin” ring $a_{conv} \sim 3.7 \cdot 10^{-4} H_p$ (see Eq. (28) and Fig. 8) between the O-loop and the walls of the magnetic tube (see Fig. 8), it is not difficult to show that the estimate of the Alfvén speed (see Eq. (32))

$$v_A \cong 4.1 \cdot 10^6 \text{ cm/s} \quad (33)$$

allows us to estimate the analytical coincidence of the rise speed v_{rise} (see Eq. (31)) and the magnetic buoyancy speed v_B :

$$(v_{rise})_{conv} \equiv (v_B)_{conv} \approx 1.4 \cdot 10^5 \text{ cm/s}, \quad (34)$$

at which for such large magnetic fields there is a significant number of rising tubes at all latitudes (see also the red lines in Figs. 12a and 11a,b).

So, for the considered case, the secondary magnetic reconnection of the flux tubes leads to the real decrease

in the magnetic field to $B \sim 10^5 \text{ G}$ at $\sim 0.8R_{Sun}$ (see Figs. 11a,b), and thereby reveals the nonzero magnetic buoyancy (see the blue lines in Fig. 11a,b). This means that for the condition of nonzero buoyancy ($\rho_{ext} \approx 0.09 \text{ g/cm}^3$) and the toroidal magnetic field of the flux tube, as well as the transverse radius of the “thin” ring $\sigma_0 \equiv a_{conv} \sim 100 \text{ km} \approx 4.5 \times 3.7 \cdot 10^{-4} H_p$ (see Fig. 11c,d), the estimate

$$v_A \cong 1.1 \cdot 10^4 \text{ cm/s} \quad (35)$$

allows us to estimate the analytical coincidence of the rise speed v_{rise} (see Eq. (31)) and the magnetic buoyancy speed v_B :

$$(v_{rise})_{conv} \equiv (v_B)_{conv} \approx 7.2 \cdot 10^2 \text{ cm/s}, \quad (36)$$

where we assume that MFTs are formed inside the disk at a height $z \sim H_p$ (see e.g. [150]). Below we consider the reason for the rising magnetic buoyancy only at low and middle latitudes.

The second part of the scenario, which is based on the remarkable idea of [155] (see also Fig. 5 in [148]), includes the generation of the magnetic field near the bottom of the convective zone (see Fig. C.1b in [10] for the holographic BL mechanism) and transfer of the toroidal field from the deep layers to the solar surface, where the efficiency of the magnetic buoyancy transfer is predetermined by the participation of two processes: macroscopic turbulent diamagnetism (see [156–163]) and rotational $\nabla\rho$ -pumping (see [155, 160, 161, 164–167]), which are also associated with the process of meridional circulation (see e.g. [107, 110, 149, 168–172] and also [150]).

Let us note some important properties of macroscopic turbulent diamagnetism. It is known that [156, 173] and

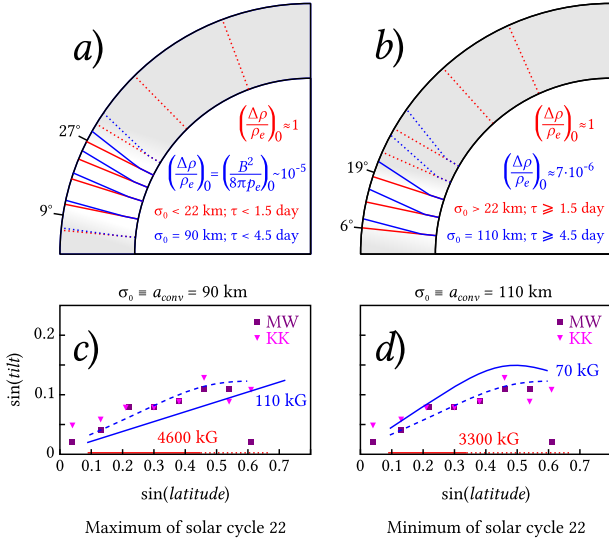


FIG. 11. (a)-(b) Flux tubes without drag of adiabatic flux ring in the superadiabatic convection zone (red lines: based on the [131] and [143] MEQ model (see also (10) in [144]), as well as on the vanBFF MEQ model (see Sect. II A)), and the trajectories of flux rings in thermal equilibrium (TEQ) incorporating drag (blue lines: based on the TEQ model of [131] and [143]; see also (5)-(10) in [144]). In (a) we use the values for the maximum of the magnetic cycle (red lines) of $(\Delta\rho/\rho_{\text{ext}})_0 = B_0^2/8\pi\rho_{\text{ext},0} \approx 1$ and $B_0 \approx 4.6 \cdot 10^7$ G for the Ω -loop with a sunspot and photons of axion origin (see Figs. 7a and 9a) and (blue lines) of $(\Delta\rho/\rho_{\text{ext}})_0 \approx 10^{-5}$ and $B_0 \approx 1.1 \cdot 10^7$ G for the Ω -loop with a sunspot and without photons of axion origin (see Fig. 9b). In (b) the values correspond to the minimum of the magnetic cycle: (red lines) $(\Delta\rho/\rho_{\text{ext}})_0 \approx 1$ and $B_0 \approx 3.3 \cdot 10^7$ G for the Ω -loop with a sunspot and photons of axion origin (see Fig. 9a) and (blue lines) $(\Delta\rho/\rho_{\text{ext}})_0 \approx 2 \cdot 10^{-6}$ and $B_0 \approx 10^7$ G for the Ω -loop with a sunspot and without photons of axion origin (see Fig. 7b). In each of the two cases, stream rings are calculated at latitudes $5^\circ, 10^\circ, 20^\circ, 30^\circ, 45^\circ, 60^\circ$. In (a) and (b) we use red and blue dotted lines of trajectories that depend on large (see Eqs. (17)-(19) in [131], where the diffusion coefficient depends on the density and k_R) and small values of the Rosseland mean opacity k_R (see (B.1) and Fig. B.3 in [10]). (c)-(d) Dependence of $\sin(\text{tilt})$ on $\sin(\text{latitude})$ in different theoretical and experimental data series. At an average value of $4.1 \cdot 10^7$ G in the tachocline, the maximum ($\sim 4.6 \cdot 10^7$ G) and minimum ($\sim 3.6 \cdot 10^7$ G) of the magnetic field of flux tubes are predetermined by two bound estimates, for example, the observational data on the variations of the magnetic field of tubes on the solar surface (see [137, 145]) and the theoretical estimates of magnetic variations in the tachocline with the EN effect (see Eqs. A.9 and A.15 in [10]). At an average value of $\sim 10^5$ G near the tachocline, the maximum ($\sim 1.1 \cdot 10^5$ G) and minimum ($\sim 7.0 \cdot 10^4$ G) of the magnetic field of flux tubes are predetermined by two analogous bound estimates. The dashed lines show the linear regressions of the average slopes of sunspot groups in the latitude range of five degrees for Mount Wilson (MW) and Kodaikanal (KK) observatories. The solid blue lines show theoretical calculations of Joy's law (see [135] and more explanation in the text).

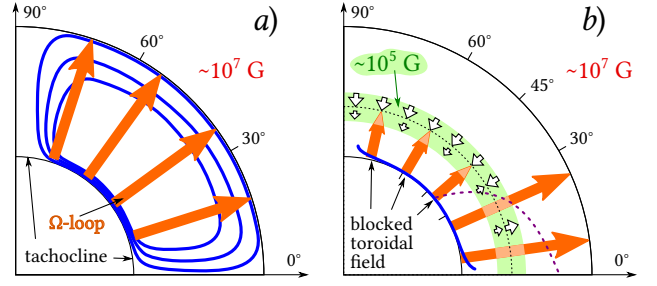


FIG. 12. Scheme of turbulent reconstruction of the toroidal magnetic field in the convective zone: (a) meridional circulation (closed blue poloidal field lines), which is generated by the toroidal field in the tachocline (thin black lines), and the magnetic buoyancy of the flux tubes (red arrows) with magnetic field $\sim 10^7$ G; (b) the joint interactions of magnetic buoyancy (red arrows) and the rotating magnetic $\nabla\rho$ -pumping (short white arrows) by means of reconnection in Ω -loop (Fig. 13) generate the total buoyancy of magnetic tubes in which the toroidal magnetic field $\sim 10^5$ G predetermines the appearance of magnetic buoyancy on the surface of the Sun only at low, and to a lesser extent at middle latitudes (see analogous Fig. 5 in [148]). The dashed curve corresponds to the zero velocity line $v_{\text{dens}}^{\text{light}}(z, \theta) = 0$, where the direction of the magnetic $\nabla\rho$ -pumping occurs.

[13] discovered the diamagnetism of inhomogeneously turbulent conducting liquids, in which the inhomogeneous magnetic field moves as a single whole. In this case the turbulent fluid, for example, with nonuniform effective diffusivity $\eta_T \approx (1/3)vl$ (see Fig. 1 in [174]; see also Fig. 13b) behaves like a diamagnetic one and carries the magnetic field with the effective velocity

$$\vec{v}_{\text{dia}} = -\frac{1}{2}\nabla\eta_T, \quad (37)$$

where l is the mixing length of turbulent pulsations, and $v = \sqrt{\langle v^2 \rangle}$ is the root-mean-square velocity of turbulent motion. The minus sign on the right in Eq. (37) shows the meaning of turbulent magnetism: it is not paramagnetic magnetism, so magnetic fields repel from regions with relatively high turbulent intensity. In other words, macroscopic turbulent plasma diamagnetism and, as a consequence, the so-called macroscopic diamagnetic effect (see [157, 158]) in the physical sense is the displacement of the averaged magnetic field B from regions with increased intensity of turbulent pulsations to regions with less developed turbulence [159, 175].

However, there is an interesting problem of the diamagnetic process caused by inhomogeneous turbulent intensity with allowance for the total nonlinearities in the magnetic field. This is due to the fact that up to the present time analytical estimates have been obtained only for the limiting cases of weak and strong magnetic fields. For example, at strong magnetic fields of flux tubes, at $B \gg B_{\text{eq}}$, the diamagnetic effect becomes almost neg-

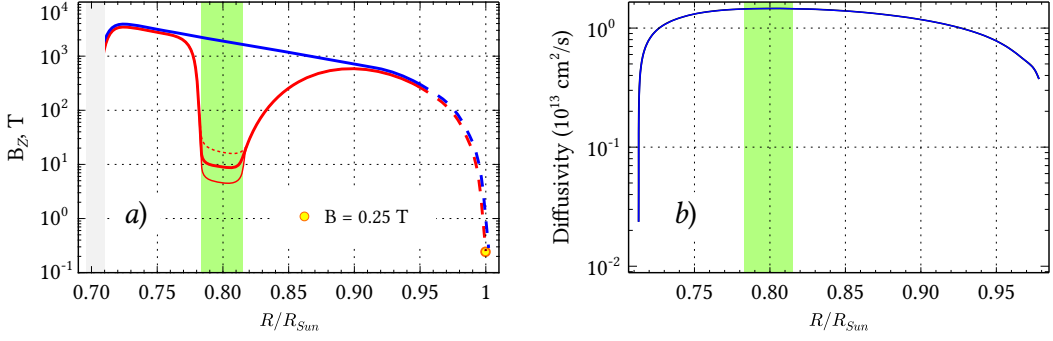


FIG. 13. **(a)** Change in the magnetic field strength B_z along the rising Ω -loop as a function of the Sun depth R/R_{Sun} in the convective zone. The blue line (see also Fig. 8 in [21, 152]) denotes admissible values for the standard solar model with diffusion of helium [94], with the initial value of the theoretical estimate of the magnetic field $B_z \approx 4 \cdot 10^7 G$ (see Eq. (2)). The red line corresponds to the cool areas inside the magnetic tube, which by means of the reconnection of the Ω -loop keeps the emerging magnetic diffusivity (green band). **(b)** Radial profile of turbulent magnetic diffusivity in the solar convection zone based on the [153] model (see also [154]). Diamagnetic pumping must be very strong near the base of the convective zone, where diffusivity almost jumps by orders of magnitude. Its gradient is the rate of descending diamagnetic pumping (see the beginning of the pumping (green band)).

ligible, in particular, strong magnetic damping of diamagnetism $\sim B^{-3}$ is obtained for super-equipartitions of fields [162], when turbulence is close to two-dimensional [156]. On the other hand, for very weak fields the diamagnetic pumping, which is predetermined by the intensity of turbulence at $B \ll B_{eq}$, is a very effective process [162].

Between the known limiting cases of weak and strong magnetic fields we are interested in the average toroidal magnetic field of a flux tube, that is $B_{tacho}^{Sun} \sim 10^5 G$, when $B \geq B_{eq}$. This is due to the fact that the secondary magnetic reconnection of the flux tubes (see Figs. 9b,d,f,g) leads to the real decrease of the magnetic field to $B \sim 10^5 G$ at $\sim 0.8 R_{Sun}$ (see the blue lines in Fig. 11a,b). This means that the real decrease in the toroidal magnetic field of the flux tube is a consequence of the formation of the secondary reconnection, as well as the important appearance of two “anti-buoyancy” effects: the downwardly directed turbulent diamagnetic transfer and the rotational effect of the magnetic $\nabla\rho$ -pumping [148, 160].

In this regard, we consider turbulence with quasi-isotropic spectral tensor [176], which is certainly the simplest representation for inhomogeneous turbulence (see Eq. (2.12) in [162]). As a consequence, the information on the spectral properties of turbulence (given by Eqs. (2.12)-(2.16) from [162]) is sufficient to reduce the expression for the average electromotive force ε (see Eq. (2.1) in [162]) to its traditional form, where only integrations over the wave number k and frequency ω remain. After such shortening it is possible to get (see [162])

$$\vec{F} = (\vec{v}_{dia} + \vec{v}_{dens}) \times \vec{B} \quad (38)$$

with the speed of turbulent diamagnetic transfer

$$\vec{v}_{dia} = -\nabla \int_0^\infty \Re_{dia}(k, \omega, B) \frac{\eta k^2 q(k, \omega, x)}{\omega^2 + \eta^2 k^4} dk d\omega, \quad (39)$$

where q stands for the local velocity spectrum, and the rate of rotational magnetic advection caused by the vertical heterogeneity of the fluid density in the convective zone, i.e. the magnetic $\nabla\rho$ -pumping effect,

$$\vec{v}_{dens} = \frac{\nabla\rho}{\rho} \int_0^\infty \Re_{dens}(k, \omega, B) \frac{\eta k^2 q(k, \omega, x)}{\omega^2 + \eta^2 k^4} dk d\omega. \quad (40)$$

The effective speeds v_{dens} and v_{dia} are consequences of the non-uniformity of density and of turbulence intensity, respectively, where the latter is attributed to the known diamagnetic pumping.

We are interested in the problem of reconstructing a strong toroidal field $\sim 10^7 G$ of flux tubes (see Figs. 12a and 13a), which by the secondary reconnection transform regions of the mean magnetic field $\sim 10^5 G$ in the convective zone (see Figs. 12b and 13a) and, thereby, allow the organization of the amazing balance between the magnetic buoyancy, turbulent diamagnetism, and the rotationally modified $\nabla\rho$ -effect. It can be shown that for the parameters $\beta = B/B_{eq} \sim 1$ and $\cos\varphi$ (see Eq. (3.5) in [162]), the speeds (39) and (40), which depend on the magnetic field B through the kernels $\Re_{dens}(\beta, \varphi)$ and $\Re_{dia}(\beta, \varphi)$ (see Eqs. (3.6) and (3.7) in [162]), have the following estimates:

$$v_{dia}^{black} \sim 1.3 \cdot 10 \text{ cm/s} \quad (41)$$

and

$$v_{dens}^{light} \sim 7.2 \cdot 10^2 \text{ cm/s}. \quad (42)$$

This raises the question of how a certain balance appears between the speeds of magnetic buoyancy (see Eq. (36) and Fig. 12), diamagnetic pumping (see Eq. (41)), and rotating densely stratified $\nabla\rho$ -pumping (see Eq. (42) and Fig. 12b),

$$(v_B^{red})_{conv} + v_{dia}^{black} + v_{dens}^{light} \cong (v_B^{red})_{conv} + v_{dens}^{light} =? \quad (43)$$

In order to consider the balance Eq. (43), it is necessary to apply the widely used approximation of the mixing length (see e.g. [111, 177–181]), which, according to [155], fully satisfies this goal. This approximation will be understood as the replacement of nonlinear terms along with time derivatives in the equations for fluctuating fields by means of τ -relaxation terms, i.e. instead of equations (3.1) and (3.9) from [155], we now have the equation of the radial speed of the toroidal field in the convection zone

$$v_{dens}^{light} = \tau \langle u^2 \rangle^\circ \frac{\nabla\rho}{\rho} \left[\phi_2(\hat{\Omega}) - \cos^2\theta \cdot \phi_1(\hat{\Omega}) \right] \approx \quad (44)$$

$$\approx 6v_p \left[\phi_2(\hat{\Omega}) - \cos^2\theta \cdot \phi_1(\hat{\Omega}) \right] = \quad (45)$$

$$= -\frac{3\kappa g}{(\gamma-1)c_p T} \left[\phi_2(\hat{\Omega}) - \cos^2\theta \cdot \phi_1(\hat{\Omega}) \right], \quad (46)$$

where $\tau \approx l/(\langle u^2 \rangle^\circ)^{1/2}$ is a typical lifetime of a convective eddy; l is the mixing length; $\langle u^2 \rangle^\circ$ is the mean intensity of fluctuating velocities for original turbulence; θ is the latitude; $e_r \nabla\rho/\rho = -e_r g/[(\gamma-1)c_p T]$, where e_r is the radial unit vector; $T \cong 1.35 \cdot 10^6 \text{ K}$ is the temperature at $0.8R_{Sun}$; $g = g_0(R_{Sun}/r)$ is the gravitational acceleration, where $g_0 = 2.74 \cdot 10^4 \text{ cm/s}^2$ is the surface value; $c_p = 3.4 \cdot 10^8 \text{ cm}^2\text{s}^{-2}\text{K}^{-1}$ (fully ionized hydrogen) is the specific heat at constant pressure; $\gamma = 5/3$ is the ratio of specific heats c_p/c_V ; $3\kappa = \tau \langle u^2 \rangle^\circ$, where $\kappa \equiv \eta_T \approx 5 \cdot 10^{13} \text{ cm}^2 \cdot \text{s}^{-1}$ is turbulent diffusivity supplied by the model of non-rotating convection zone [106, 116, 153, 182, 183] (see also Fig. 1 in [174]) and the mixing length relation $\langle u^2 \rangle^\circ = -\nabla\Delta T l^2 g/(4T)$, where the $\nabla\Delta T$ is superadiabatic temperature gradient; $v_p = (1/6)\tau \langle u^2 \rangle^\circ (\nabla\rho/\rho)$ is the velocity of the magnetic field transfer caused by the density gradient (see Eq. (36) in [160]); $\hat{\Omega} = Co = 2\tau\Omega$ is the Coriolis number (reciprocal of the Rossby number), where Ω is the rotation speed, τ is the turnover time, and the functions

$$\phi_n(\hat{\Omega}) = (1/8)I_n(\Omega, k, \omega) \quad (47)$$

(see I_1 and I_2 in Eqs. (3.12) and (3.21) in [155]) are

$$\phi_1(\hat{\Omega}) = \frac{1}{4\hat{\Omega}^2} \left[-3 + \frac{\hat{\Omega}^2 + 1}{\hat{\Omega}} \arctan \hat{\Omega} \right], \quad (48)$$

$$\phi_2(\hat{\Omega}) = \frac{1}{8\hat{\Omega}^2} \left[1 + \frac{\hat{\Omega}^2 - 1}{\hat{\Omega}} \arctan \hat{\Omega} \right] \quad (49)$$

(see also analogous Eq. (19) and Fig. 2 in [163]), which describe the rotational effect on turbulent convection.

According to [184], the rotational effect on the flow can be measured with the local Coriolis number $\hat{\Omega} = Co = 2\tau\Omega$, especially if τ is estimated on the basis of the theory of mixing length, which predicts values of $\hat{\Omega}$ reaching more than 10 in the deep layers (see e.g. [185–188]). However, on the other hand, according to [184], the question of whether there are such deep layers of solar and stellar convection zones or not is still open.

At the same time, we showed that this rotating magnetic $\nabla\rho$ -pumping appears precisely in the deep layers (through reconnection of the Ω -loop (see Figs. 12b and 13) at middle and low latitudes, where the influence of the rotational gradient causes the upward magnetic pumping. The direction of the magnetic $\nabla\rho$ -pumping (up or down, see Fig. 12b) is susceptible to the sign of the factor in Eqs. (48) - (49), which depends on the polar angle (colatitude) and the behavior of the Coriolis number functions in the convection zone.

Below we show that the estimate of the Coriolis number for solar convection in the deep layer should be $\hat{\Omega} \approx 20$. As a consequence of (47)-(49), the following values are assumed for this quantity:

$$\phi_1 \cong 0.0171, \quad \phi_2 \cong 0.0098, \quad (50)$$

at which the radial velocity (44) of toroidal field transport changes the sign at the latitude $\theta^* = \arccos \sqrt{\varphi_2/\varphi_1} \cong 41^\circ$, being negative (downward) for $\theta > \theta^*$ and positive (upward) for $\theta < \theta^*$. Using (46), we find that the value of the radial velocity in the convective zone v_{dens}^{light} (see Eqs. (44)-(46)) near low latitudes (e.g. $\theta^* = \arccos(0.985) \cong 10^\circ$; see also Fig. 12b) almost completely coincides with the value of the speed (42), which was previously calculated with the help of the magnetic field B in the kernel $\mathfrak{R}_{dens}(\beta, \varphi)$.

This means that the balance of the magnetic buoyancy (see Eq. (36) and Fig. 12) and rotating density-stratified $\nabla\rho$ -pumping (see Eq. (42) and Fig. 12b) provides both the process of blocking the magnetic buoyancy at high latitudes,

$$\uparrow (v_B^{red})_{conv} + \downarrow v_{dens}^{light} \leq 0 \quad \text{at high latitudes}, \quad (51)$$

and the process of lifting MFTs from the base of the convective zone to the solar surface at low latitudes,

$$\uparrow (v_B^{red})_{conv} + \uparrow v_{dens}^{light} > 0 \quad \text{at lower latitudes,} \quad (52)$$

which are simultaneously predetermined by the following rise time value:

$$(\tau_B^{red})_{conv} \sim \frac{z_0}{(v_B^{red})_{conv} + v_{dens}^{light}} \leq 4.5 \text{ day,} \quad (53)$$

where $z_0 \approx 0.1 H_p$ is the length of the magnetic line at $0.8R_{Sun}$ (see the green band in Fig. 13). Here we must remember that magnetic $\nabla\rho$ -pumping of plasma from the azimuthal field through the formation of the Ω -loop is repeated again and again (see Fig. 7 and Fig. 4 in [106]). Moreover, our theoretical estimates of the rise time of the Ω -loop are in good agreement with the experimental observations by [189], who mention the repeated appearance of new Ω -loops with an interval of 5-8 days, which simultaneously indicates the continuing convective pumping of plasma.

We have shown above that the sunspots – the dark magnetic regions occurring at low latitudes on the surface of the Sun (see Fig. 12) – are indicators of the magnetic field generated not with the help of the dynamo mechanism (this is very important!), which does not exist here, but with the help of the holographic BL mechanism as components of the model of solar antidymano (see Fig. C.1b in [10]). Hence, the question arises as to how the sunspots originating from magnetic buoyancy on the surface only at low and, to a lesser extent, middle latitudes do not contradict the known observational data of the tilt angle of Joy’s law (see Fig. 11c,d).

Hence, it is very interesting that the holographic BL mechanism, which is a satisfactory alternative theory against the action of the dynamo, predetermines not only the generation of sunspots themselves on the surface at low and middle latitudes (see Fig. 12), but their coincidence with the observed slope angle of Joy’s law, where, as a consequence, the average angle of inclination of bipolar sunspots increases with latitude (see Fig. 11c,d). This is due to the fact that strong toroidal magnetic fields in the overshoot tachocline are generated by the holographic BL mechanism (see Fig. C.1 in [10]), and bipolar magnetic tubes are created by lifting Ω -loops caused by magnetic buoyancy. As a result, these ascending Ω -loops, according to [143], will be bent (towards the pole; see also Fig. 14) by the Coriolis force, so that they eventually appear on the surface of the Sun with the tilt angle (see Fig. 11).

Using the magnetic field strength near the bottom of the convective zone of the order of $10^5 G$ at $0.8R_{Sun}$ (see Figs. 12b and 13a), we find that the Coriolis force plays a dominant role, and the MFTs, starting from the bottom at low latitudes, deviate by $0.8R_{Sun}$ (see Figs. 11a,b and 14) and appear on the surface of the Sun at low and middle latitudes, located in the direction of the poles as sunspots. It is obvious that since the time of radiation diffusion of the flux tube (see Fig. 11a) is related to Eq. (53),

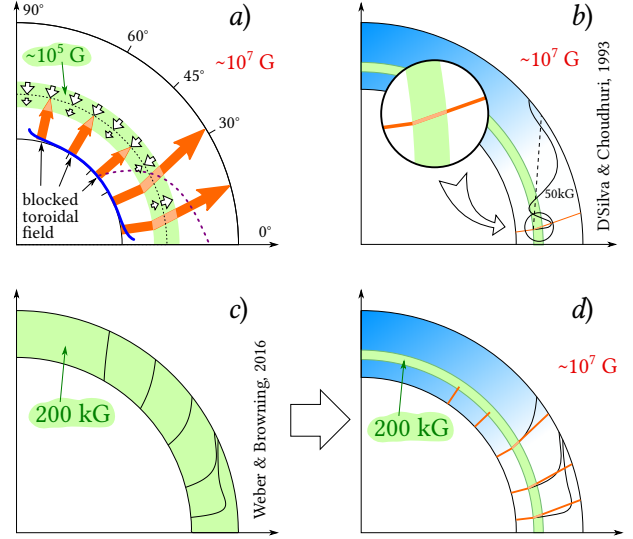


FIG. 14. (a) Interactions of magnetic buoyancy (red arrows) and rotating magnetic $\nabla\rho$ -pumping (short white arrows) generate the total buoyancy of magnetic tubes in which the toroidal magnetic field $\sim 10^7 G$ predetermines the appearance of magnetic buoyancy by using the dominant Coriolis force in $\nabla\rho$ -pumping with $\sim 10^5 G$ (see Fig. 12b), which ultimately generates a curved upward loop on the surface of the Sun with a slope in the lower and, to a lesser extent, middle latitudes (see Fig. 11a,b). (b) According to [144], the trajectory of stream loops with 50 kG in the $\xi - \theta$ plane realized at latitude 5° in the lower part of the convective zone. The dashed line shows the contour of constant angular momentum. A streaming ring of 50 kG, realized at 5° , also oscillates around this contour and comes out to a high latitude. The streaming ring “hugs” the contour of constant angular momentum, which is almost parallel to the axis of rotation. When we use Fig. 14b, which is the modified Fig. 14 from [144], the inset shows the trajectory of the tubes with $\sim 10^7 G$, which, ultimately, by $\nabla\rho$ -pumping with $\sim 5 \cdot 10^4 G$ (green line) generates a curved ascending loop on the solar surface with a tilt in the lower latitudes. At the same time, the flow ring “hugs” the contour of constant angular momentum, which is not parallel to the axis of rotation, which, of course, will be in good agreement with the observations of the slope angle of Joy’s law (see Fig. 11c,d). (c) According to [121], the trajectories of tubes initiated at $0.75R_{Sun}$ (see Case T0 (black lines)) can cause (by means of induced Coriolis forces) tubes to move horizontally outwards to smaller layers at lower latitudes, and deeper layers at higher latitudes, caused by the direction of the flow backward. (d) When we use Fig. 14c, which is the modified Fig. 6 from [121], the trajectory of flux tubes with $\sim 10^7 G$ ultimately, by $\nabla\rho$ -pumping with $\sim 5 \cdot 10^4 G$ (green line, see also Fig. 14d) generates a curved ascending loop on the solar surface with a tilt in the lower latitudes.

$$(\tau_B^{red})_{conv} \equiv (\tau_d)_{conv} \leq 4.5 \text{ day,} \quad (54)$$

using the equations (32), (35), (36), it is possible to estimate the average width of the “ring” of the MFT:

$$a_{conv} \sim 100 \text{ km}. \quad (55)$$

Here we are interested in the relationship between the speed of magnetic buoyancy, $(v_B^{red})_{conv}$, and the average width of the “ring” σ_0 , which is identical to a_{conv} based on the vanBFF model (see Sect. II A). Using Eq. (23) from [131]

$$\frac{(v_B^{red})_{conv}}{4.8 \cdot 10^3 \text{ cm/s}} \equiv u'_t = \left(\frac{4\pi}{C_D} \cdot \frac{\sigma_0}{R_{Sun}} \cdot \frac{(\Delta\rho/\rho_{ext})_0}{2 \cdot 10^{-6}} \right)^{1/2}, \quad (56)$$

which connects the cross-section of the magnetic tube “ring” $\sigma_0 \equiv a_{conv}$ (see Eq. (21)) with the thermal velocity in dimensionless coordinates (see analogous Table 1 in [131]), it is not difficult to show that for $(\Delta\rho/\rho_{ext})_0 \sim 10^{-5}$ (or equivalently at $B_0 = v_A(4\pi\rho)^{1/2} \sim 10^5 \text{ G}$) the magnetic buoyancy values $(v_B^{red})_{conv}/4.8 \cdot 10^3 \text{ cm/s} \equiv u'_t \approx 0.15$ and $\sigma_0 \equiv a_{conv} \sim 100 \text{ km}$ remarkably coincide with the corresponding values of Eqs. (36) and (55), respectively.

III. SUMMARY AND OUTLOOK

The main result of the theory of magnetic flux tubes is the properties of dark matter axions identical to solar axions, the modulations of which are controlled by the anticorrelated 11-year modulation of the asymmetric dark matter (ADM) density in the solar interior [10]:

1. The existence of anchored flux tubes with 10^7 G in the overshoot tachocline is a consequence of the fundamental properties of the holographic principle of quantum gravity, one of which (unlike the dynamo action!) generates a strong toroidal field in the tachocline with the help of the holographic BL mechanism (see Fig. 1b and C.1b in [10]).
2. The theory of the almost empty anchored magnetic flux tubes with $B \sim 10^7 \text{ G}$ is the result of the formation of the magnetic O-loop (through the primary reconnection) inside the MFT in the lower part of the convective zone, which efficiently converts the solar axions and high-energy photons from the radiation zone into photons of axion origin and axions of photonic origin, respectively. The appearance of the axions of photonic origin is, on the one hand, the manifestation of a “ring” of a strong magnetic tube due to convective heating $(dQ/dt)_2$ (Fig. 8). On the other hand, it leads to a remarkable result of the “disappearance” of Parker’s convective heat transport, and consequently, to the rise of the temperature in the lower part of the magnetic tube. At the same time, the Parker-Biermann cooling effect is preserved in the convective zone, when a free path opens for the photons of axion origin

from the tachocline to the photosphere! From here it is possible, for example, to obtain a solution to the problem of corona heating [10].

The existence of magnetic buoyancy of flux tubes from the tachocline to the surface of the Sun is a consequence of the primary trajectory formation through the so-called universal model of van Ballegooijen-Fan-Fisher (vanBFF model), which is determined by the equation $dQ/dt = (dQ/dt)_1 + (dQ/dt)_2$. The first term $(dQ/dt)_1$ defines the average temperature gradient between the lower convective zone and the overshoot (see Eq. 27), which deviates significantly from the radiation equilibrium, which in turn suggests the presence of a nonzero divergence of the heating radiation flux. The second term $(dQ/dt)_2$ represents the convective diffuse radiation passing through a flux tube due to temperature differences between the tube and the ambient plasma, radiation thermal conductivity, and the mean width of the magnetic tube “ring” (see Eq. (28) and the area of the magnetic tube “ring” $2\pi r a_{conv}$, where r is the magnetic tube radius).

It was shown that at strong fields of $\sim 10^7 \text{ G}$, which are determined by the thermomagnetic EN effect (as a consequence of the holographic principle of quantum gravity), the external gas pressure is almost equal to the magnetic pressure between the tube and the ambient plasma. This leads to the virtually empty magnetic tube: $dQ/dt \approx (dQ/dt)_2 \gg (dQ/dt)_1$. It means that solar axions, which are magnetically converted from the high-energy photons of the radiation zone, on the one hand, directly suppress the radiation heating in the convective zone, and on the other hand, initiate an increase in convective heating by a sharp decrease in the average width of the magnetic tube “ring”. As a result, the convective heating $(dQ/dt)_2$ strongly dominates over the radiation heating $(dQ/dt)_1$.

This way we apply a new analysis of the universal vanBFF model, where the calculated values such as the magnetic flux Φ , the rise time τ_d and the rise speed $(v_{rise})_{conv}$ of the MFT to the surface of the Sun, do not contradict the known observational data.

3. The existence of the magnetic buoyancy of flux tubes on the surface of the Sun is a consequence of the formation of a secondary trajectory by magnetic reconnection with $B \sim 10^5 \text{ G}$ (see blue lines in Fig. 11a,b), at which, on the one hand, the formation of the rotating density-stratified $\nabla\rho$ -pumping with $B \sim 10^5 \text{ G}$ near the tachocline (see green bands in Figs. 12b and 13a) provides the process of blocking magnetic buoyancy at high latitudes, and on the other hand, it predetermines the existence of the dominant Coriolis force in $\nabla\rho$ -pumping with $B \sim 10^5 \text{ G}$, which ultimately generates an arched

ascending loop on the surface of the Sun with a tilt in the lower and, to a lesser extent, middle latitudes (see Figs. 11 and 14a).

4. The basic properties of an almost empty magnetic tube (see Figs. 5 and 8), characterizing thin radii of the cross-section ($\sigma_0 \equiv a_{conv} \sim 20 \text{ km}$) and strong magnetic fields $\sim 10^7 \text{ G}$, do not contradict the existence of a thin flux tube, since a virtually empty magnetic tube, unlike thin flux tubes, has not only strong magnetic fields, but also the width of the “ring” ($\sigma_0 \equiv a_{conv} \sim 100 \text{ km}$) of the MFT between the surface of the thick O-loop and the wall of the tube (see Figs. 5 and 8). It means that it is not the thin flux tubes with $\sim 10^5 \text{ G}$ near the tachocline (see green bands in Figs. 12b and 13a) that serve as a basis for the role of the Coriolis force at a certain latitude of the rising tilt in the direction of the active region. Therefore, the mean width of the

magnetic tube “ring” (see Fig. 8) and the arched ascending loop of the magnetic field lines (see the tilt angle of Joy’s law in Fig. 11c,d and Fig. 14) are allowed.

5. The averaged theoretical estimates of the magnetic cycle of flux tubes are practically identical to the observational (averaged) data of the tilt angle of Joy’s law (see Fig. 11c,d).

In the future, we will apply the results of the theory of magnetic tubes in strong fields not only to the Sun and a black hole, which was partially obtained in our work [10], but also consider its implications for the case of the well-known paradigm of fazzball complementarity in a black hole, which “challenges” the standard models of the central engine of a black hole for gamma-ray bursts and suggests a common physical mechanism behind GRBs, which indicates the magnetar central engine of GRBs.

-
- [1] M. Rempel and R. Schlichenmaier, *Living Rev. Solar Phys.* **8** (2011).
 - [2] E. N. Parker, *Astrophys. J.* **121**, 491 (1955).
 - [3] L. Biermann, *Vierteljahrsschrift Astron. Gesellsch.* **76**, 194 (1941).
 - [4] E. N. Parker, *Astrophys. J.* **230**, 905 (1979).
 - [5] H. Alfvén, *Nature* **150**, 405 (1942).
 - [6] E. N. Parker, *Astrophysical Journal* **189**, 563 (1974).
 - [7] E. N. Parker, *Astrophysical Journal* **190**, 429 (1974).
 - [8] E. N. Parker, *Solar Physics* **36**, 249–274 (1974).
 - [9] E. N. Parker, *Astrophysical Journal* **215**, 370 (1977).
 - [10] V. D. Rusov, I. V. Sharph, V. P. Smolyar, M. V. Eingorn, and M. E. Beglaryan, *Physics of the Dark Universe* **31**, 100746 (2021).
 - [11] A. V. Etingshausen and W. Nernst, *Wied. Ann.* **29**, 343 (1886).
 - [12] E. H. Sondheimer, *Proceedings of the Royal Society of London. Series A, Mathematical and Physical Sciences* **193**, 484 (1948).
 - [13] L. J. Spitzer, *Physics of Fully Ionized Gases* (John Wiley & Sons, Inc., New York, 1956).
 - [14] Y. B. Kim and M. J. Stephen, in *Superconductivity*, Vol. 2, edited by R. Parks (Dekker, New York, 1969).
 - [15] W. A. Fowler, G. R. Burbidge, and E. M. Burbidge, *Astrophysical Journal Supplement* **2**, 167 (1955).
 - [16] S. Couvidat, S. Turck-Chièze, and A. G. Kosovichev, *The Astrophysical Journal* **599**, 1434 (2003).
 - [17] T. G. Cowling, *Monthly Notices of the Royal Astronomical Society* **94**, 39 (1933).
 - [18] S. Sanchez, A. Fournier, and J. Aubert, *Astrophysical Journal* **781**, 8 (2014).
 - [19] L. J. Spitzer, *Physics of Fully Ionized Gases*, 2nd ed. (Interscience Publishers, John Wiley & Sons, New York, 1962).
 - [20] L. J. Spitzer, *Physics of Fully Ionized Gases*, 2nd ed. (Dover Publications, Inc., Mineola, New York, 2006).
 - [21] V. Rusov, M. Eingorn, I. Sharph, V. Smolyar, and M. Beglaryan (2015), [arXiv:1508.03836 \[astro-ph.SR\]](https://arxiv.org/abs/1508.03836).
 - [22] G. G. Raffelt, *Phys. Lett.* **592**, 391 (2004).
 - [23] G. G. Raffelt, *Lect. Notes Phys.* **741**, 51 (2008), [arXiv:hep-ph/0611350](https://arxiv.org/abs/hep-ph/0611350).
 - [24] R. D. Peccei and H. R. Quinn, *Physical Review Letters* **38**, 1440–1443 (1977).
 - [25] R. D. Peccei and H. R. Quinn, *Phys. Rev. D* **16**, 1791 (1977).
 - [26] M. Kawasaki and K. Nakayama, *Annual Review of Nuclear and Particle Science* **63**, 69–95 (2013).
 - [27] D. J. Marsh, *Physics Reports* **643**, 1 (2016), axion cosmology.
 - [28] L. Di Luzio, M. Giannotti, E. Nardi, and L. Visinelli, *Physics Reports* **870**, 1–117 (2020).
 - [29] P. Sikivie, *Reviews of Modern Physics* **93**, 015004 (2021).
 - [30] A. Schneider, R. E. Smith, and D. Reed, *Monthly Notices of the Royal Astronomical Society* **433**, 1573–1587 (2013).
 - [31] J.-W. Hsueh, W. Enzi, S. Vegetti, M. W. Auger, C. D. Fassnacht, G. Despali, L. V. E. Koopmans, and J. P. McKean, *Monthly Notices of the Royal Astronomical Society* **492**, 3047 (2019).
 - [32] D. Gilman, S. Birrer, A. Nierenberg, T. Treu, X. Du, and A. Benson, *Monthly Notices of the Royal Astronomical Society* **491**, 6077 (2019).
 - [33] R. T. Co and K. Harigaya, *Phys. Rev. Lett.* **124**, 111602 (2020).
 - [34] P. Carenza, T. Fischer, M. Giannotti, G. Guo, G. Martínez-Pinedo, and A. Mirizzi, *Journal of Cosmology and Astroparticle Physics* **2019** (10), 016–016.
 - [35] A. D. Goulding, J. E. Greene, R. Bezanson, J. Greco, S. Johnson, A. Leauthaud, Y. Matsuoka, E. Medezinski, and A. M. Price-Whelan, *Publications of the Astronomical Society of Japan* **70**, S37 (2018), [arXiv:1706.07436 \[astro-ph.GA\]](https://arxiv.org/abs/1706.07436).
 - [36] A. C. Vincent, P. Scott, and A. Serenelli, *Journal of Cosmology and Astroparticle Physics* **11**, 007, [arXiv:1605.06502 \[hep-ph\]](https://arxiv.org/abs/1605.06502).

- [37] CAST Collaboration, *Nature Physics* **13**, 584–590 (2017).
- [38] E. Armengaud, D. Attié, S. Basso, P. Brun, N. Bykovskiy, J. Carmona, J. Castel, S. Cebrián, M. Cicoli, M. Civitani, and et al., *Journal of Cosmology and Astroparticle Physics* **2019** (06), 047–047.
- [39] K. M. Backes, D. A. Palken, S. A. Kenany, B. M. Brubaker, S. B. Cahn, A. Droster, G. C. Hilton, S. Ghosh, H. Jackson, S. K. Lamoreaux, and et al., *Nature* **590**, 238 (2021).
- [40] B. M. Brubaker, L. Zhong, S. K. Lamoreaux, K. W. Lehnert, and K. A. van Bibber, *Physical Review D* **96**, 123008 (2017).
- [41] C. Boutan, M. Jones, B. H. LaRoque, N. S. Oblath, R. Cervantes, N. Du, N. Force, S. Kimes, R. Ottens, L. J. Rosenberg, and et al., *Physical Review Letters* **121**, 261302 (2018).
- [42] P. Sikivie, *Physical Review Letters* **51**, 1415–1417 (1983).
- [43] *Particle Dark Matter: Observations, Models and Searches* (Cambridge University Press, 2010).
- [44] E. W. Kolb and M. S. Turner, *The early universe*, Vol. 69 (1990).
- [45] In contrast to the (incomplete) Standard Model, the Higgs-boson here is supposed to have integer weak isospin, which is consistent with the experimental data on its decay channels [190]. It is considered as a bound state of W^+ and W^- bosons – the particles with weak isospin of 1. Since the weak isospin of gauge bosons is equal to unity, the bound state can have a weak isospin of 2, 1 or 0. The state with zero isospin obviously cannot take part in weak interactions. It has zero electric charge and does not consist of strongly interacting particles. Therefore, such a state can interact only gravitationally. On the other hand, it has all the theoretical properties of the Higgs boson. For example, in the model of multiparticle fields, the spontaneous symmetry breaking is NOT postulated as in the Standard Model (see [47]), but is obtained as a result of the dynamic equations of the model, as a result of which it has a nonzero vacuum value. Due to these properties, it can be considered as a candidate for dark matter [46, 47].
- [46] K. K. Merkotan, T. M. Zelentsova, N. O. Chudak, D. A. Ptashynskiy, V. V. Urbanevich, O. S. Potienko, V. V. Voitenko, O. D. Berezovskiy, I. V. Sharph, and V. D. Rusov, *Journal of Physical Studies* **22**, 10.30970/jps.22.3001 (2018), (in Ukrainian).
- [47] D. A. Ptashynskiy, T. M. Zelentsova, N. O. Chudak, K. K. Merkotan, O. S. Potienko, V. V. Voitenko, O. D. Berezovskiy, V. V. Opyatyuk, O. V. Zharova, T. V. Yushkevich, I. V. Sharph, and V. D. Rusov, *Ukrainian Journal of Physics* **64**, 732 (2019).
- [48] S. B. Giddings and A. Strominger, *Nuclear Physics B* **307**, 854 (1988).
- [49] S. Coleman, *Nuclear Physics B* **310**, 643 (1988).
- [50] G. Gilbert, *Nuclear Physics B* **328**, 159 (1989).
- [51] D. Harlow and H. Ooguri, *Phys. Rev. Lett.* **122**, 191601 (2019).
- [52] D. Harlow and H. Ooguri, Symmetries in quantum field theory and quantum gravity (2019), [arXiv:1810.05338](https://arxiv.org/abs/1810.05338) [hep-th].
- [53] M. V. Eingorn and V. D. Rusov, *Foundations of Physics* **45**, 875 (2015), [arXiv:1309.5761](https://arxiv.org/abs/1309.5761) [gr-qc].
- [54] K. Harigaya, in *Zooming in on Axions in the Early Universe* (CERN, 2020).
- [55] R. T. Co, N. Fernandez, A. Ghalsasi, L. J. Hall, and K. Harigaya, *Journal of High Energy Physics* **2021**, 17 (2021).
- [56] Planck Collaboration, *A&A* **641**, A6 (2020).
- [57] In this case, neutrinos and helioseismic information thus complement each other, especially when the presence of particles such as axions at the maximum luminosity of the Sun, and particles such as the Higgs ADM at the minimum luminosity of the Sun, affects the transfer of heat within the interior of the Sun. Therefore, the maximum and minimum of neutrino fluxes can simultaneously solve a very complex “problem of solar composition”, or otherwise called “the problem of solar abundance”, which is associated with the solar cycle. Most important here is that the neutrino flux from the subdominant CNO cycle is linearly dependent on the metallicity (Z) of the solar core (see e.g. [191–194]). It means that the modulation of solar abundance, with high metallicity at the solar maximum ($Z \sim 0.0170$ with $Z/X = 0.023$ [58]) and low metallicity at the solar minimum ($Z \sim 0.0133$ with $Z/X = 0.0178$ [195]), is in good agreement with the deviation of the radial sound speed profile $\delta c_s/c_s = (c_{s,obs} - c_{s,th})/c_{s,obs}$ inside the Sun (Fig. 4), which consists of two related models: for the maximum luminosity of axions (Fig. 4a) and for the minimum luminosity of axions, which is associated with the maximum luminosity of Higgs ADM (Fig. 4b).
- [58] N. Grevesse and A. J. Sauval, *Space Science Reviews* **85**, 161 (1998).
- [59] N. Vinyoles, A. Serenelli, F. L. Villante, S. Basu, J. Redondo, and J. Isern, *Journal of Cosmology and Astroparticle Physics* **10**, 015, [arXiv:1501.01639](https://arxiv.org/abs/1501.01639) [astro-ph.SR].
- [60] A. C. Vincent, P. Scott, and A. Serenelli, *Physical Review Letters* **114**, 081302 (2015), [arXiv:1411.6626](https://arxiv.org/abs/1411.6626) [hep-ph].
- [61] A. C. Vincent, A. Serenelli, and P. Scott, *Journal of Cosmology and Astroparticle Physics* **8**, 040, [arXiv:1504.04378](https://arxiv.org/abs/1504.04378) [hep-ph].
- [62] S. Degl’Innocenti, W. A. Dziembowski, G. Fiorentini, and B. Ricci, *Astroparticle Physics* **7**, 77 (1997), [astro-ph/9612053](https://arxiv.org/abs/astro-ph/9612053).
- [63] G. Fiorentini, B. Ricci, and F. Villante, *Physics Letters B* **503**, 121 (2001).
- [64] Planck Collaboration, *A&A* **594**, A13 (2016).
- [65] C. Patrignani and Particle Data Group, *Chinese Physics C* **40**, 100001 (2016), 11. STATUS OF HIGGS BOSON PHYSICS.
- [66] S. Nussinov, *Physics Letters B* **165**, 55–58 (1985).
- [67] R. Chivukula and T. P. Walker, *Nuclear Physics B* **329**, 445–463 (1990).
- [68] S. Barr, R. Sekhar Chivukula, and E. Farhi, *Physics Letters B* **241**, 387–391 (1990).
- [69] D. B. Kaplan, *Physical Review Letters* **68**, 741–743 (1992).
- [70] D. Hooper, J. March-Russell, and S. M. West, *Physics Letters B* **605**, 228–236 (2005).
- [71] D. E. Kaplan, M. A. Luty, and K. M. Zurek, *Physical Review D* **79**, 115016 (2009).
- [72] H. Davoudiasl and R. N. Mohapatra, *New Journal of Physics* **14**, 095011 (2012).
- [73] K. Petraki and R. R. Volkas, *International Journal of Modern Physics A* **28**, 1330028 (2013), [arXiv:1305.4939](https://arxiv.org/abs/1305.4939)

- [hep-ph].
- [74] K. M. Zurek, *Physics Reports* **537**, 91 (2014), [arXiv:1308.0338 \[hep-ph\]](#).
- [75] P. W. Graham, I. G. Irastorza, S. K. Lamoreaux, A. Lindner, and K. A. van Bibber, *Annual Review of Nuclear and Particle Science* **65**, 485–514 (2015).
- [76] D. H. Hathaway, *Living Reviews in Solar Physics* **12**, 4 (2015).
- [77] T. G. Cowling, The solar system (The University of Chicago Press, Chicago, 1953) Chap. The Sun, p. 532.
- [78] G. E. Hale, *Astrophysical Journal* **28**, 315 (1908).
- [79] J. Evershed, *Monthly Notices of the Royal Astronomical Society* **69**, 454 (1909).
- [80] S. K. Solanki, *The Astronomy and Astrophysics Review* **11**, 153 (2003).
- [81] J. M. Borrero and K. Ichimoto, *Living Reviews in Solar Physics* **8**, 4 (2011).
- [82] S. K. Tiwari, M. van Noort, S. K. Solanki, and A. Lagg, *A&A* **583**, A119 (2015).
- [83] S. E. Pozuelo, L. R. B. Rubio, and J. de la Cruz Rodríguez, *The Astrophysical Journal* **803**, 93 (2015).
- [84] G. Guerrero and P. J. Käpylä, *A&A* **533**, A40 (2011).
- [85] N. J. Nelson, B. P. Brown, A. S. Brun, M. S. Miesch, and J. Toomre, *The Astrophysical Journal* **762**, 73 (2013).
- [86] P. J. Käpylä, M. J. Mantere, E. Cole, J. Warnecke, and A. Brandenburg, *The Astrophysical Journal* **778**, 41 (2013).
- [87] A. C. Birch, D. C. Braun, K. D. Leka, G. Barnes, and B. Javornik, *The Astrophysical Journal* **762**, 131 (2013).
- [88] A. C. Birch, H. Schunker, D. C. Braun, R. Cameron, L. Gizon, B. Löptien, and M. Rempel, *Science Advances* **2**, 10.1126/sciadv.1600557 (2016).
- [89] R. Stein, *Living Rev. Solar Phys.* **9**, 4 (2012).
- [90] S. M. Hanasoge, T. L. D. Jr, and M. L. DeRosa, *The Astrophysical Journal Letters* **712**, L98 (2010).
- [91] S. M. Hanasoge, T. L. Duvall, and K. R. Sreenivasan, *Proceedings of the National Academy of Sciences* **109**, 11928 (2012).
- [92] S. Hanasoge, M. S. Miesch, M. Roth, J. Schou, M. Schüssler, and M. J. Thompson, *Space Science Reviews* **196**, 79 (2015).
- [93] L. Gizon and A. C. Birch, *Proceedings of the National Academy of Sciences* **109**, 11896 (2012).
- [94] J. Bahcall and M. Pinsonneault, *Rev. Mod. Phys.* **64**, 885 (1992).
- [95] A. Kolmogorov, *Akademiia Nauk SSSR Doklady* **30**, 301 (1941).
- [96] A. N. Kolmogorov, *Soviet Physics Uspekhi* **10**, 734 (1968).
- [97] A. N. Kolmogorov, *Proceedings of the Royal Society of London A: Mathematical, Physical and Engineering Sciences* **434**, 9 (1991).
- [98] E. N. Parker, *The Astrophysics Journal* **433**, 867 (1994).
- [99] S. Jabbari, *Origin of solar surface activity and sunspots*, Ph.D. thesis, Stockholm University, Faculty of Science, Department of Astronomy. NORDITA. (2016), uRN: urn:nbn:se:su:diva-128774, OAI: oai:DiVA.org:su-128774, DiVA, id: diva2:916647.
- [100] A. W. Baggaley, C. F. Barenghi, A. Shukurov, and K. Subramanian, *Phys. Rev. E* **80**, 055301 (2009).
- [101] N. F. Loureiro, D. A. Uzdensky, A. A. Schekochihin, S. C. Cowley, and T. A. Yousef, *Monthly Notices of the Royal Astronomical Society: Letters* **399**, L146 (2009).
- [102] Y.-M. Huang and A. Bhattacharjee, *Physics of Plasmas* **17**, 062104 (2010).
- [103] A. Beresnyak, *Astrophysical Journal* **834**, 47 (2017), [arXiv:1301.7424 \[astro-ph.SR\]](#).
- [104] H. C. Spruit, A. M. Title, and A. A. Van Ballegoijen, *Solar Physics* **110**, 115 (1987).
- [105] P. R. Wilson, P. S. McIntosh, and H. B. Snodgrass, *Solar Physics* **127**, 1 (1990).
- [106] E. N. Parker, *Space Sci. Rev.* **122**, 15 (2009).
- [107] H. C. Spruit and A. A. van Ballegoijen, *Astronomy and Astrophysics* **106**, 58 (1982).
- [108] E. N. Parker, *Astrophysical Journal* **198**, 205 (1975).
- [109] E. N. Parker, *Cosmical magnetic fields: Their origin and their activity* (Oxford, Clarendon Press, 1979) p. 858.
- [110] A. A. van Ballegoijen, *Astronomy and Astrophysics* **113**, 99 (1982).
- [111] E. Böhm-Vitense, *Zeitschrift fuer Astrophysik* **46**, 108 (1958).
- [112] H. C. Spruit, *Magnetic Flux Tubes and Transport of Heat*, Ph.D. thesis, Ph. D. Thesis, Utrecht University (1977).
- [113] A. S. Brun, M. S. Miesch, and J. Toomre, *The Astrophysical Journal* **742**, 79 (2011).
- [114] R. Smolec and P. Moskalik, *Acta Astronomica* **58**, 193 (2008), [arXiv:0809.1979](#).
- [115] R. Smolec and P. Moskalik, *A&A* **524**, A40 (2010).
- [116] H. Spruit, *Solar Physics* **34**, 277 (1974).
- [117] J. Christensen-Dalsgaard, M. J. P. F. G. Monteiro, and M. J. Thompson, *Monthly Notices of the Royal Astronomical Society* **276**, 283 (1995).
- [118] J. Christensen-Dalsgaard, M. J. P. F. G. Monteiro, M. Rempel, and M. J. Thompson, *Monthly Notices of the Royal Astronomical Society* **414**, 1158 (2011).
- [119] Y. Fan and G. Fisher, *Solar Phys.* **166**, 17 (1996).
- [120] M. A. Weber and Y. Fan, *Solar Physics* **290**, 1295 (2015), [arXiv:1503.08034 \[astro-ph.SR\]](#).
- [121] M. A. Weber and M. K. Browning, *The Astrophysical Journal* **827**, 95 (2016).
- [122] Y. Fan, G. H. Fisher, and E. E. Deluca, *Astrophysical Journal* **405**, 390 (1993).
- [123] C. Zwaan, *Annual Review of Astronomy and Astrophysics* **25**, 83 (1987).
- [124] J. E. Bailey, G. A. Rochau, R. C. Mancini, C. A. Iglesias, J. J. Macfarlane, I. E. Golovkin, C. Blancard, P. Cosse, and G. Faussurier, *Physics of Plasmas* **16**, 058101 (2009).
- [125] S. Ilonidis, J. Zhao, and A. Kosovichev, *Science* **333**, 993 (2011).
- [126] S. Ilonidis, J. Zhao, and A. Kosovichev, *Science* **336**, 296 (2012).
- [127] S. Ilonidis, J. Zhao, and T. Hartlep, *The Astrophysical Journal* **777**, 138 (2013).
- [128] A. G. Kosovichev, J. Zhao, and S. Ilonidis, *ArXiv e-prints* (2016), [arXiv:1607.04987 \[astro-ph.SR\]](#).
- [129] S. Jabbari, A. Brandenburg, D. Mitra, N. Kleeorin, and I. Rogachevskii, *Monthly Notices of the Royal Astronomical Society* **459**, 4046 (2016).
- [130] K. Petrovay and L. van Driel-Gesztelyi, *Solar Physics* **176**, 249 (1997).
- [131] A. R. Choudhuri and P. A. Gilman, *Astrophysical Journal* **316**, 788 (1987).
- [132] M. K. Browning, M. A. Weber, G. Chabrier, and A. P. Massey, *Astrophysical Journal* **818**, 189 (2016),

- arXiv:1512.05692 [astro-ph.SR].
- [133] M. Dasi-Espuig, S. K. Solanki, N. A. Krivova, R. Cameron, and T. Peñuela, *Astronomy and Astrophysics* **518**, A7 (2010), arXiv:1005.1774 [astro-ph.SR].
- [134] M. Dasi-Espuig, Solanki, S. K., Krivova, N. A., Cameron, R., and Peñuela, T., *A&A* **556**, C3 (2013).
- [135] V. G. Ivanov, *Geomagnetism and Aeronomy* **52**, 999 (2012).
- [136] B. H. McClintock and A. A. Norton, *Solar Physics* **287**, 215 (2013), arXiv:1305.3205 [astro-ph.SR].
- [137] A. A. Pevtsov, L. Bertello, A. G. Tlatov, A. Kilcik, Y. A. Nagovitsyn, and E. W. Cliver, *Solar Physics* **289**, 593 (2014), arXiv:1301.5935 [astro-ph.SR].
- [138] K. A. Tlatova, V. V. Vasil'eva, and A. A. Pevtsov, *Geomagnetism and Aeronomy* **55**, 896 (2015).
- [139] Senthamizh Pavai, V., Arlt, R., Dasi-Espuig, M., Krivova, N. A., and Solanki, S. K., *A&A* **584**, A73 (2015).
- [140] T. Baranyi, *Monthly Notices of the Royal Astronomical Society* **447**, 1857 (2015).
- [141] Y.-M. Wang, R. C. Colaninno, T. Baranyi, and J. Li, *Astrophysical Journal* **798**, 50 (2015), arXiv:1412.2329 [astro-ph.SR].
- [142] Y.-M. Wang, *Space Science Reviews* **210**, 351 (2017).
- [143] A. R. Choudhuri, *Solar Physics* **123**, 217 (1989).
- [144] S. D'Silva and A. R. Choudhuri, *Astronomy and Astrophysics* **272**, 621 (1993).
- [145] A. A. Pevtsov, Y. A. Nagovitsyn, A. G. Tlatov, and A. L. Rybak, *The Astrophysical Journal Letters* **742**, L36 (2011).
- [146] M. Schüssler and M. Rempel, in *From Solar Min to Max: Half a Solar Cycle with SOHO*, ESA Special Publication, Vol. 508, edited by A. Wilson (2002) pp. 499–506.
- [147] Y. Fan, *Living Rev. Solar Phys.* **6**, 4 (2009).
- [148] V. N. Krivodubskij, *Astronomische Nachrichten* **326**, 61 (2005).
- [149] A. A. van Ballegoijen and A. R. Choudhuri, *Astrophysical Journal* **333**, 965 (1988).
- [150] S. A. Khaibrakhmanov, A. E. Dudorov, S. Y. Parfenov, and A. M. Sobolev, *Monthly Notices of the RAS* **464**, 586 (2017), arXiv:1609.03969 [astro-ph.SR].
- [151] B. Roberts and P. Murdin, Solar photospheric magnetic flux tubes: theory (2001), encyclopedia of Astronomy and Astrophysics, Institute of Physics, Nature Publishing Group, London.
- [152] V. Rusov, M. Eingorn, I. Sharph, V. Smolyar, and M. Beglaryan (2019), arXiv:1908.06042 [astro-ph.SR].
- [153] M. Stix and D. Skaley, *Astronomy and Astrophysics* **232**, 234 (1990).
- [154] M. Stix, *The Sun: An Introduction* (Springer, Berlin, 2004).
- [155] L. L. Kichatinov, *Astronomy and Astrophysics* **243**, 483 (1991).
- [156] Y. B. Zel'dovich, *Sov. Phys. JETP* **4**, 460 (1957).
- [157] K.-H. Rädler, *Zeitschrift für Naturforschung A* **23**, 1841 (1968).
- [158] K.-H. Rädler, *Zeitschrift für Naturforschung A* **23**, 1841 (1968).
- [159] S. I. Vainshtein, Y. B. Zel'dovich, and A. A. Ruzmaikin, *The Turbulent Dynamo in Astrophysics* (Nauka, Moscow, 1980).
- [160] S. I. Vainshtein and L. L. Kichatinov, *Geophysical & Astrophysical Fluid Dynamics* **24**, 273 (1983).
- [161] M. Stix, *The Sun. An Introduction, XIII*, 390 pp. 192 figs.. Springer-Verlag Berlin Heidelberg New York. Also *Astronomy and Astrophysics Library* (1989) p. 192.
- [162] L. L. Kichatinov and G. Ruediger, *Astronomy and Astrophysics* **260**, 494 (1992).
- [163] L. L. Kichatinov and A. A. Nepomnyashchikh, *Advances in Space Research* **58**, 1554 (2016), solar Dynamo Frontiers.
- [164] E. M. Drobyshevski and V. S. Yuferev, *Journal of Fluid Mechanics* **65**, 33–44 (1974).
- [165] S. Vainshtein, *Magnetic Fields in Space* (Nauka, Moscow, 1983).
- [166] M. Ossendrijver, M. Stix, A. Brandenburg, and G. Rüdiger, *A&A* **394**, 735 (2002).
- [167] L. L. Kichatinov and S. V. Olemskoy, *Solar Physics* **276**, 3 (2012), arXiv:1108.3138 [astro-ph.SR].
- [168] A. E. Dudorov and A. K. Kirillov, *Byulletin Solnechnye Dannye Akademii Nauk SSSR* **1985**, 85 (1986).
- [169] W. Y.-M., N. R. Sheeley, Jr., and A. G. Nash, *Astrophysical Journal* **383**, 431 (1991).
- [170] A. R. Choudhuri, M. Schüssler, and M. Dikpati, *Astronomy and Astrophysics* **303**, L29 (1995).
- [171] P. Caligari, F. Moreno-Insertis, and M. Schussler, *Astrophysical Journal* **441**, 886 (1995).
- [172] D. Nandy and A. R. Choudhuri, *Science* **296**, 1671 (2002).
- [173] Y. B. Zel'dovich, *Sov. Phys. JETP* **31**, 154 (1956).
- [174] L. L. Kichatinov and G. Rüdiger, *Astronomische Nachrichten* **329**, 372 (2008).
- [175] F. Krause and K.-H. Raedler, *Organic Photonics and Photovoltaics* (1980).
- [176] L. L. Kichatinov, *Geophysical & Astrophysical Fluid Dynamics* **38**, 273–292 (1987).
- [177] P. Bradshaw, *Nature* **249**, 135 (1974).
- [178] D. O. Gough, *Astrophysical Journal* **214**, 196 (1977).
- [179] D. Gough, in *Problems of Stellar Convection*, Lecture Notes in Physics, Berlin Springer Verlag, Vol. 71, edited by E. A. Spiegel and J.-P. Zahn (1977).
- [180] A. J. Barker, A. M. Dempsey, and Y. Lithwick, *The Astrophysical Journal* **791**, 13 (2014).
- [181] A. Brandenburg, *The Astrophysical Journal* **832**, 6 (2016).
- [182] D. O. Gough and N. O. Weiss, *Monthly Notices of the Royal Astronomical Society* **176**, 589 (1976).
- [183] B. B. Karak, J. Jiang, M. S. Miesch, P. Charbonneau, and A. R. Choudhuri, *Space Science Reviews* **186**, 561 (2014).
- [184] Käpylä, P. J., Käpylä, M. J., and Brandenburg, A., *A&A* **570**, A43 (2014).
- [185] M. Ossendrijver, *Astronomy and Astrophysics* **11**, 287 (2003).
- [186] A. Brandenburg and K. Subramanian, *Physics Reports* **417**, 1 (2005).
- [187] P. Käpylä, *Astronomische Nachrichten* **332**, 43 (2011).
- [188] P. Käpylä, M. Mantere, and A. Brandenburg, *Astronomische Nachrichten* **332**, 883 (2011).
- [189] V. Gaizauskas, K. L. Harvey, J. W. Harvey, and C. Zwaan, *Astrophysical Journal* **265**, 1056 (1983).
- [190] Particle Data Group, *Progress of Theoretical and Experimental Physics* **2020**, 10.1093/ptep/ptaa104 (2020), 083C01.
- [191] G. D. O. Gann, *AIP Conference Proceedings* **1666**, 090003 (2015).
- [192] The Borexino Collaboration, *Nature* **587**, 577 (2020).
- [193] BOREXINO Collaboration, *The European Physical*

- Journal C* **80**, 1091 (2020).
- [194] N. Tapia-Arellano and S. Horiuchi, *Physical Review D* **103**, 123016 (2021).
- [195] M. Asplund, N. Grevesse, A. J. Sauval, and P. Scott, *Annual Review of Astron and Astrophys* **47**, 481 (2009), arXiv:0909.0948 [astro-ph.SR].